# Rehomogenization of nodal cross sections via modal synthesis of neutron spectrum changes

Gamarino, Matteo; Dall'Osso, Aldo; Lathouwers, Danny; Kloosterman, Jan Leen

**DOI**
10.1080/00295639.2017.1417214

**Publication date**
2018

**Document Version**
Final published version

**Published in**
Nuclear Science and Engineering

**Citation (APA)**
Gamarino, M., Dall'Osso, A., Lathouwers, D., & Kloosterman, J. L. (2018). Rehomogenization of nodal cross sections via modal synthesis of neutron spectrum changes. *Nuclear Science and Engineering*, *190*(1), 1-30. https://doi.org/10.1080/00295639.2017.1417214

Nuclear Science and Engineering

ISSN: 0029-5639 (Print) 1943-748X (Online) Journal homepage: http://www.tandfonline.com/loi/unse20

# Rehomogenization of Nodal Cross Sections via Modal Synthesis of Neutron Spectrum Changes

Matteo Gamarino, Aldo Dall'Osso, Danny Lathouwers & Jan Leen Kloosterman

**To cite this article:** Matteo Gamarino, Aldo Dall'Osso, Danny Lathouwers & Jan Leen Kloosterman (2018) Rehomogenization of Nodal Cross Sections via Modal Synthesis of Neutron Spectrum Changes, Nuclear Science and Engineering, 190:1, 1-30, DOI: 10.1080/00295639.2017.1417214

**To link to this article:** https://doi.org/10.1080/00295639.2017.1417214



Published online: 06 Mar 2018.

NUCLEAR SCIENCE AND ENGINEERING · VOLUME 190 · 1–30 · APRIL 2018

DOI: https://doi.org/10.1080/00295639.2017.1417214



# Rehomogenization of Nodal Cross Sections via Modal Synthesis of Neutron Spectrum Changes

Matteo Gamarino,[a]* Aldo Dall'Osso,[b] Danny Lathouwers,[a] and Jan Leen Kloosterman[a]

[a]*Delft University of Technology, Department of Radiation, Science and Technology, Mekelweg 15, 2629 JB, Delft, The Netherlands*
[b]*AREVA NP, Tour AREVA, 92084 Paris La Défense Cedex, France*

Received August 29, 2017
Accepted for Publication December 11, 2017

**Abstract** — *Nodal diffusion is currently the preferred neutronics model for industrial reactor core calculations, which use few-group cross-section libraries generated via standard assembly homogenization. The infinite-medium flux-weighted cross sections fail to capture the spectral effects triggered in the core environment by nonreflective boundary conditions at the fuel-assembly edges. This poses a serious limitation to the numerical simulation of current- and next-generation reactor cores, characterized by strong interassembly heterogeneity.*

*Recently, a spectral rehomogenization method has been developed at AREVA NP. This approach consists of an on-the-fly modal synthesis of the spectrum variation between the environmental and infinite-medium conditions. It uses information coming from both the nodal simulation and the lattice transport calculation performed to compute the standard cross sections. The accuracy of the spectral corrections depends on the choice of the basis and weighting functions for the expansion and on the definition of a realistic energy distribution of the neutron leakage. In this paper, we focus on the first aspect. Two tracks are researched: a combination of analytical functions (with a physically justified mode) and a mathematical approach building upon the Proper Orthogonal Decomposition. The method is applied to relevant pressurized-water-reactor benchmark problems. We show that the accuracy of the cross sections is significantly improved at reasonably low computational cost and memory requirement. Several aspects of the methodology are discussed, such as the interplay with space-dependent corrections. We demonstrate that this approach can model not only the spectral interactions between dissimilar neighbor assemblies but also the spectral effects due to different physical conditions (namely, multiplicative properties) in the environment and in the infinite medium.*

**Keywords** — *Nodal diffusion, homogenization, spectral correction.*

**Note** — *Some figures may be in color only in the electronic version.*

## I. INTRODUCTION

Nodal diffusion methods are nowadays one of the most common computational tools for reactor core design and operation.[1,2] Few-group cross sections used in nodal codes for three-dimensional full-core simulations derive from standard energy collapsing and spatial homogenization performed during preliminary lattice transport calculations with reflective boundary conditions (also referred to as infinite-medium conditions).[3] Their preparation involves a set of reference cross sections (interpolated at proper temperature and dilution and self-shielded) in a very fine number of energy groups and a reference condensation spectrum computed in the most detailed geometry. During the

*E-mail: m.gamarino@tudelft.nl

core calculation, the cross-section dependence on the local physical conditions (such as burnup, moderator density, fuel temperature, and diluted-boron concentration) is resolved by the interpolation from parameterized tables as a function of instantaneous and history variables. The major weakness of this methodology is that the infinite-medium neutron flux used for cross-section weighting at the single-assembly calculation stage does not account for the environmental effects. These arise when the assembly is located in the reactor core due to typically nonreflective boundary conditions. Hence, the equivalence between the nodal representation and the real global solution from transport can be guaranteed only if the flux distribution inside the assembly is close to the infinite-medium one (that is, if the assembly is surrounded by assemblies of the same type in a large medium compared to the neutron mean free path). However, this condition is seldom met in modern reactor core layouts, characterized by strongly heterogeneous configurations aiming to reduce the neutron leakage, to optimize the core-power distribution, and to maximize the fuel exploitation. Typical examples are fuel loading patterns combining low-enriched uranium and mixed oxide (MOX) assemblies; reflector boundaries; layouts with local, strong burnable absorbers; elaborate insertion schemes of control mechanisms; and depleted-assembly shuffling strategies. With these increasingly widespread complex designs, the nodal cross sections built by the standard homogenization paradigm could fail to reproduce accurate estimates of the reaction rates and multiplication factor. Eventually, even with default adjustments in the construction of parameterized tables (such as criticality by the fundamental-buckling correction), high-fidelity simulations of water reactors with environment-independent homogenization parameters are only possible for fresh fuel at start-up in weakly heterogeneous systems. Therefore, the core-environment conditions need to be modeled to provide more accurate inputs for nodal solvers.

Heterogeneity-induced effects have an impact on the neutron flux distribution in both space and energy. For example, Fig. 1a shows the infinite-medium spatially averaged neutron spectra (normalized to unity) in two adjacent $UO_2$ and MOX assemblies at zero burnup. Figure 1b displays the variation of the spectrum (in percent) in the two fuel bundles in the core environment. The perturbation in the neutron distribution is significant, especially at thermal energies.

Even if the spatial and spectral effects are tightly coupled, for the sake of simplicity they are often addressed separately by reactor analysis methods. In order to deal with the former, Smith introduced an efficient iterative method for cross-section homogenization.[4] Recently, a two-dimensional (2-D) submesh-based rehomogenization scheme has been adopted in Studsvik's SIMULATE nodal code,[5] and a spatial rehomogenization method has been developed at AREVA NP (Ref. 6). Moreover, in most nodal codes a spatial intraassembly dependence of the nodal cross sections is imposed to capture burnup and isotopic-inventory gradients,[7,8] and possibly, to model design heterogeneity.[9]

In the present work we focus on spectral effects. A number of techniques have been proposed in the past to

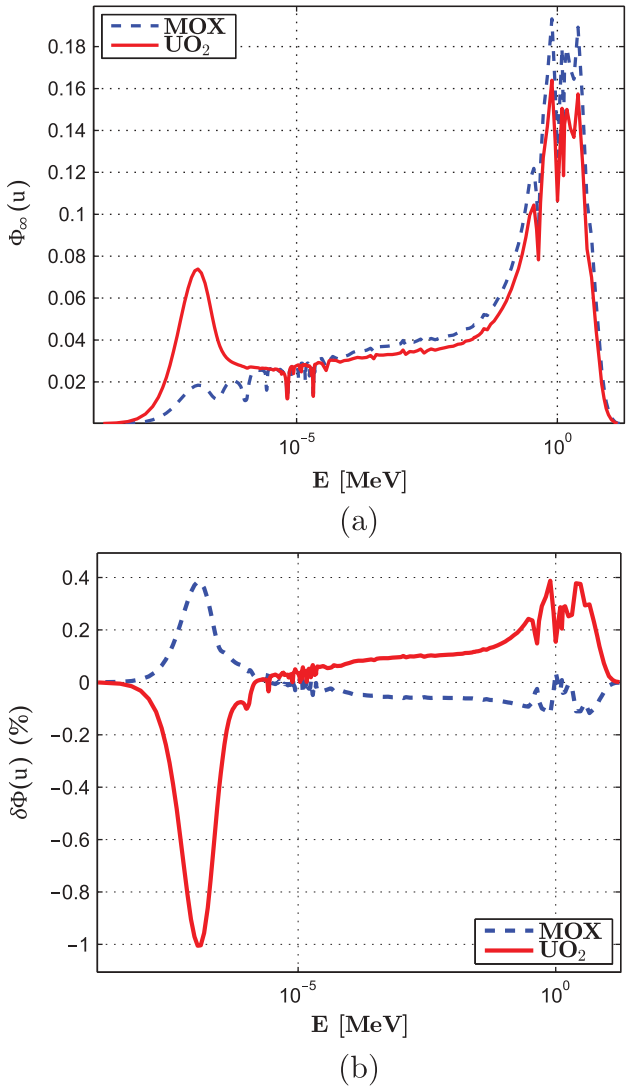


Fig. 1. Spectral effects at a $UO_2$-MOX interface: (a) infinite-medium assembly-averaged spectra (normalized to unity) per unit lethargy $u$ and (b) variation of the spectrum in the two assemblies in the real environment (in units of percent).

correct the single-assembly cross sections for these. For instance, considerable effort has been put into approaches tabulating the impact of dissimilar neighbor nodes. One of them, presented by Palmtag, applies an empirical correlation accounting for local spectral interactions.[10] This method, originally developed for $UO_2$-MOX interfaces, relies on the observations that the fractional change in the fast-group cross sections is proportional to the leakage-to-removal ratio of fast neutrons and that the relative variation in spectral index (raised to a power close to 1) accurately matches the relative variations in the cross sections. In a similar approach proposed later called the Leakage Feedback Method,[11] the cross-section functionalization is extended to the leakage fractions of both groups, and a separate formulation is proposed for peripheral fuel assemblies facing the reflector.

Rahnema and Nichita proposed a method to interpolate the corrections on the nodal cross sections and discontinuity factors as a function of the surface current-to-flux ratio.[12] The tabulated corrections are precomputed during the lattice-calculation phase via parametric assembly simulations with varying albedo boundary conditions. Recently, a variant of this approach has been proposed.[13] When using this kind of method, additional lattice calculations are required to include the auxiliary albedo parameter(s) in the cross-section libraries. Clarno and Adams employed a spatial superposition of colorsets in order to reduce the number of extra calculations,[14] whereas Rahnema and McKinley developed a high-order cross-section homogenization method that does not demand to perform parametric lattice calculations.[15] The latter approach is based on high-order boundary-condition perturbation theory[16,17] and requires two infinite-medium adjoint functions precomputed as additional homogenization parameters. Among the other spectral-correction approaches recently developed, we mention the recondensation method[18] and the semiheterogeneous transport-embedded approach.[19]

In this paper we present AREVA NP's spectral rehomogenization method. This approach consists of estimating the difference between the environmental and infinite-medium node-averaged spectra. This is done at the core calculation level by means of a limited set of known modal components in the domain of energy. The spectrum variation modal expansion is solved by Galerkin or Petrov-Galerkin projection of the local fine-group neutron balance equation over a set of weighting operators. The energy condensation defects are thus evaluated on the fly and added to the nodal cross sections provided by the standard lattice calculation.

Since the earliest formulation of the method,[20] original work has been done in the definition of its two pillars: the modal synthesis of the environmental spectrum and a consistent model for the neutron leakage spectral distribution. In the present work we mainly focus on the first subject. Two tracks for the search of the trial and test functions are investigated and compared: a Proper Orthogonal Decomposition (POD) approach and a more conventional strategy based on the use of analytical functions (Chebyshev polynomials) and of a physically justified mode (the neutron fission-emission spectrum). The methodology is validated by numerical simulations of few assembly-configuration samples representative of the spectral effects of the environment observable in a reactor core. The main implementation features of the method are outlined, and its approximations and limitations are discussed. We point out the main advantages and shortcomings of the two modal approaches in terms of both accuracy and computational efficiency. An analysis is presented on the interplay between the spectral rehomogenization method and the critical-buckling spectrum correction, typically imposed at the cross-section library preparation stage to reduce the homogenization defect. We also address the complementarity with space-dependent cross-section corrections. Finally, preliminary results of a model for the neutron leakage spectrum are shown.

The paper is structured as follows. Section II presents the rehomogenization method with the latest developments. Section III discusses various sets of basis and weighting operators for the modal synthesis of the spectrum change. The implementation of the rehomogenization approach in the light water reactor (LWR) two-step procedure is detailed. Section IV shows numerical results for some pressurized water reactor (PWR) sample problems. Section V addresses several aspects of the methodology. Conclusive remarks and recommendations for future work follow in Sec. VI.

## II. DESCRIPTION OF THE METHOD

The spectral rehomogenization method considered in this work is part of a more general cross-section correction model aiming to reproduce environmental effects of various natures. In previous work,[21] an analytical expression was determined for the few-group nodal cross section homogenized ($h$) in the real environment, $\Sigma^{(h)}_{G,env}$. This reads as follows:

$$\Sigma^{(h)}_{G,env} = \Sigma^{(h)}_{G,\infty} + \delta\Sigma^{(r)}_{G} + \delta\Sigma^{(xs)}_{G} , \qquad (1)$$

where

$\Sigma_{G,\infty}^{(h)}$ = single-assembly cross section (interpolated from the libraries at the current values of the local state parameters)

$\delta\Sigma_G^{(r)}$ = homogenization defect due to the flux variation $\delta\Phi_g(\mathbf{r},E)$ between the real environment and the infinite-medium conditions

$\delta\Sigma_G^{(xs)}$ = homogenization error due to the variations in the cross-section distribution caused by the depletion in the real environment (we encompassed in this term the corrections described in Refs. 7 and 8).

In the same work,[21] a flux factorization was used to decouple the spatial and spectral components of the homogenization-flux defect. We showed that the following approximation holds:

$$\delta\Sigma_G^{(r)} \approx \delta\Sigma_G^{(spat)} + \delta\Sigma_G^{(spectr)} + \delta\Sigma_G^{(cross)} \ , \tag{2}$$

where the cross correction $\delta\Sigma_G^{(cross)}$ represents the contribution of mixed space-energy terms. This component of the homogenization error accounts for the fact that the spatial and spectral effects of the environment cannot be rigorously superposed due to their inherent nonseparability.

According to our derivation, the spectral cross-section correction $\delta\Sigma_{x,G}$ for the reaction type $x$ and the coarse group $G$ in a generic node can be estimated as follows (from now on we drop the superscript *spectr* for the sake of lightness of the notation):

$$\delta\Sigma_{x,G} = \frac{1}{\bar{\Phi}_G}\int_{E_G^-}^{E_G^+} dE\,\Sigma_{x,G}^{\infty}(E)\delta\Phi_G(E) \ , \tag{3}$$

where

$E_G^+,\ E_G^-$ = $G$'th-group upper and lower energy boundaries, respectively

$\Sigma_{x,G}^{\infty}(E)$ = distribution in energy of the infinite-medium spatially averaged cross section within group $G$

$\bar{\Phi}_G$ = nodal integral flux

$\delta\Phi_G(E)$ = variation of the node-averaged neutron energy spectrum due to environmental effects.

The nodal flux $\bar{\Phi}_G$ is simply defined as

$$\bar{\Phi}_G = \frac{1}{V}\int_V d\vec{r}\Phi_G(\vec{r}) \ , \tag{4}$$

where $V$ is the volume of the node. We solve for $\delta\Phi_G(E)$ by a modal-expansion approach. In order to find an expression for this variable, we consider the neutron continuous-energy balance equation in the real environment for a generic homogenized node:

$$\begin{aligned}\Sigma_{t,env}(E)\Phi_{env}(E) + L_{env}(E) &= \frac{\chi_{env}(E)}{k_{eff}}\int_0^{\infty} dE'\nu\Sigma_{f,env}(E')\Phi_{env}(E') \\ &+ \int_0^{\infty} dE'\Sigma_{s,env}(E'\rightarrow E)\Phi_{env}(E') \ ,\end{aligned} \tag{5}$$

where $\Phi_{env}(E)$ and $L_{env}(E)$ represent the neutron spectrum and the leakage energy distribution in the environmental conditions, respectively. The meaning of the remaining symbols corresponds to common notation in reactor physics literature.[2] One of the main approximations of the method is to neglect the dependence of the cross-section distributions on the environment [i.e., $\Sigma_{x,env}(E) \approx \Sigma_{x,\infty}(E)$]. This assessment will be the subject of a thorough discussion in Sec. V.A.1 (from now on, the subscript referring to the type of environment is dropped from the cross-section notation). We replace the energy $E$ by a lethargy-like quantity $u$, defined separately within each coarse energy group $G$ as

$$u = \frac{\ln\left(\frac{E}{E_G^-}\right)}{\ln\left(\frac{E_G^+}{E_G^-}\right)} \ . \tag{6}$$

This change of variable is made in order to ease the search of the basis and test functions. The quantity $u$ is bounded between 0 and 1 in each macrogroup. It is remarked that this ad hoc variable does not correspond to the definition of lethargy commonly found in reactor physics textbooks [i.e., $u = \ln(E_0/E)$, with $E_0$ usually set to 10 MeV for reactor calculations]; in our case, $u$ increases with $E$. As most nodal codes employed for LWR analysis make use of two energy groups, we consider here a two-group framework ($N_G = 2$), with $E_1^+ = 19.6$ MeV, $E_1^- \equiv E_2^+ = 0.625$ eV, and $E_2^- = 1.1\times10^{-10}$ MeV. However, the methodology can be extended to an arbitrary number of groups. In the following, we use the notation $u_1$ and $u_2$ to indicate the lethargy domain within the fast and thermal coarse groups, respectively.

Replacing $E$ with $u$ and moving to the two-group formulation, Eq. (5) can be rewritten, for group $G$, as

$$\Sigma_{t,G}(u)\Phi_{env,G}(u) + L_{env,G}(u) = \sum_{G'=1}^{2}\left(\frac{\chi_G(u)}{k_{eff}}\int_0^1 du'\nu\Sigma_{f,G'}(u')\Phi_{env,G'}(u') + \int_0^1 du'\Sigma_{s,G'\to G}(u'\to u)\Phi_{env,G'}(u')\right). \quad (7)$$

In each coarse group, we define the environmental spectrum as the sum of the reference distribution in the infinite-medium conditions and of the sought spectrum variation $\delta\Phi_G(u)$:

$$\Phi_{env,G}(u) = \bar{\Phi}_G\varphi_{\infty,G}(u) + \delta\Phi_G(u)\,. \quad (8)$$

In Eq. (8), the $G$'th group single-assembly spectrum $\varphi_{\infty,G}(u)$ is normalized to unity, and $\delta\Phi_G(u)$ has zero average. Therefore, the following normalization condition is satisfied:

$$\int_0^1 du\Phi_{env,G}(u) = \bar{\Phi}_G\,. \quad (9)$$

The spectrum difference is expanded in terms of the modal components $Q_{G,i}(u)$:

$$\delta\Phi_G(u) = \sum_{i=1}^{N_{Q_G}}\alpha_{G,i}Q_{G,i}(u)\ , \quad (10)$$

where $N_{Q_G}$ is the group-dependent number of basis functions. We choose basis functions having zero average within each coarse group to satisfy the condition of Eq. (9).

We formulate $L_{env,G}(u)$ as

$$L_{env,G}(u) = \bar{L}_G f_{L,G}(u)\ , \quad (11)$$

where $f_{L,G}(u)$ is a form function describing the spectral behavior of the multigroup leakage in the real environment and $\bar{L}_G$ is the node-averaged integral leakage. The latter can be computed as follows:

$$\bar{L}_G = \sum_{d=x,y,z}\frac{J_{G,d+} - J_{G,d-}}{\Delta d}\ , \quad (12)$$

where

$\Delta d$ = node width along direction $d$

$J_{G,d+}$, $J_{G,d-}$ = surface-averaged currents at the node boundaries $d+$ and $d-$.

An estimate of the few-group quantities $\bar{\Phi}_G$ and $\bar{L}_G$ and of the multiplication factor $k_{eff}$ appearing in Eqs. (7), (8), and (11) is known from the nodal solution. We assume that these best-estimate quantities satisfy the balance equation integrated in energy (this is another approximation of the method).

If the leakage energy shape is known, the expansion coefficients $\alpha_{G,i}$ are the only unknowns of the spectral rehomogenization problem. In order to solve for them, we set a system of algebraic equations applying a standard weighted-residual technique to Eq. (7). After substitution of Eqs. (8), (10), and (11), Eq. (7) is projected over the test functions $W_{G,j}(u)$ (with $j = 1,\cdots,N_{Q_G}$) and then integrated over $u$ within each coarse group. The use of a fully mathematical approach to determine the equations of the system is justified by the local distortion of shape observed in the computed spectrum perturbation when physically justified conditions are imposed. These include the continuity of the environmental spectrum and of its first derivative at the boundary between the two energy groups, and the condition $\delta\Phi(u=1) = 0$ within the fast group. After projection and some algebraic manipulation, the term corresponding to the reaction rate $x$ reads as

$$\int_0^1 duW_{G,j}(u)\Sigma_{x,G}(u)\Phi_{env,G}(u) = \bar{\Phi}_G h_{R,x,G,j} + \sum_{i=1}^{N_{Q_G}}\alpha_{G,i}h_{V,x,G,i,j}\ , \quad (13)$$

with the rehomogenization parameters $h_{R,x,G,j}$ and $h_{V,x,G,i,j}$ defined as

$$h_{R,x,G,j} = \int_0^1 duW_{G,j}(u)\Sigma_{x,G}(u)\varphi_{\infty,G}(u) \quad (14a)$$

and

$$h_{V,x,G,i,j} = \int_0^1 duW_{G,j}(u)\Sigma_{x,G}(u)Q_{G,i}(u) \quad (14b)$$

The reference coefficients $h_{R,x,G,j}$ carry the information of the (reference) collapsing spectrum computed in the infinite lattice, whereas the variational coefficients $h_{V,x,G,i,j}$ are defined in terms of the components of the spectrum perturbation. With the aforementioned

assumption $\Sigma^{env}_{x,G}(u) \approx \Sigma^{\infty}_{x,G}(u)$, the coefficients in Eq. (14) only depend on infinite-medium quantities ($\Sigma_{x,G}$, $\varphi_{\infty,G}$), known at the lattice-calculation level, and on the predefined basis and weighting functions of the modal expansion. There is no dependence on environmental quantities. Therefore, they can be easily computed during the cross-section library preparation phase.

Applying the above procedure to the terms appearing in Eq. (7), the rehomogenization problem can be cast in the following form:

$$\bar{\Phi}_G h_{R,t,G,j} + \sum_{i=1}^{N_{Q_G}} \alpha_{G,i} h_{V,t,G,i,j} + c_{G,j}\bar{L}_G = \sum_{G'=1}^{2} \bar{\Phi}_{G'}\left(h_{R,s,G'\to G,j} + \frac{\chi_{G,j}}{k_{eff}} h_{R,f,G'}\right) + \sum_{G'=1}^{2}\sum_{i=1}^{N_{Q_{G'}}} \alpha_{G',i}\left(h_{V,s,G'\to G,i,j} + \frac{\chi_{G,j}}{k_{eff}} h_{V,f,G',i}\right), \quad (15)$$

where $c_{G,j}$, $\chi_{G,j}$, and the coefficients $h_R$ and $h_V$ are the rehomogenization parameters corresponding to the fine-group neutron leakage, fission-emission spectrum, and various reaction rates. The variables in Eq. (15) are formulated as follows:

$$c_{G,j} = \int_0^1 du W_{G,j}(u) f_{L,G}(u) , \quad (16a)$$

$$\chi_{G,j} = \int_0^1 du W_{G,j}(u) \chi_G(u) , \quad (16b)$$

$$h_{R,t,G,j} = \int_0^1 du W_{G,j}(u) \Sigma_{t,G}(u) \varphi_{\infty,G}(u) , \quad (16c)$$

$$h_{V,t,G,i,j} = \int_0^1 du W_{G,j}(u) \Sigma_{t,G}(u) Q_{G,i}(u) , \quad (16d)$$

$$h_{R,f,G} = \int_0^1 du \nu\Sigma_{f,G}(u) \varphi_{\infty,G}(u) , \quad (16e)$$

$$h_{V,f,G,i} = \int_0^1 du \nu\Sigma_{f,G}(u) Q_{G,i}(u) , \quad (16f)$$

$$h_{R,s,G'\to G,j} = \int_0^1 du W_{G,j}(u) \int_0^1 du' \Sigma_{s,G'\to G}(u'\to u) \varphi_{\infty,G'}(u') , \quad (16g)$$

and

$$h_{V,s,G'\to G,i,j} = \int_0^1 du W_{G,j}(u) \int_0^1 du' \Sigma_{s,G'\to G}(u'\to u) Q_{G',i}(u') . \quad (16h)$$

Equation (15) reduces to a $2N_{Q_G} \times 2N_{Q_G}$ [$N_G N_{Q_G} \times N_G N_{Q_G}$ in a more general form when $N_{Q_G}$ is the same in each coarse group] linear system that can be solved for each homogenized region following a nonlinear iteration of the nodal solution. The quantities $\bar{\Phi}_G$, $\bar{L}_G$, and $k_{eff}$ are taken from the prior, partially converged power iteration of the eigenvalue calculation, whereas the precomputed rehomogenization coefficients defined in Eq. (16) are interpolated from the cross-section libraries as a function of the local conditions. No additional lattice calculation is needed, neither when updating the cross sections throughout the nodal simulation nor at the library level.

After determining the coefficients $\alpha_{G,i}$, the spectral cross-section correction for the reaction type $x$ in a generic node can be computed as

$$\delta\Sigma_{x,G} = \frac{1}{\bar{\Phi}_G}\int_0^1 du \Sigma^{\infty}_{x,G}(u)\delta\Phi_G(u) = \frac{1}{\bar{\Phi}_G}\sum_{i=1}^{N_{Q_G}} \alpha_{G,i} h_{V,x,G,i,0} , \quad (17)$$

where we have used the fact that $W_{G,0}(u) = 1$.

In the derivation presented here, no assumption is made about the spectral distribution of the neutron leakage $L_{env,G}(u)$. In order for the rehomogenization model to be applicable, the definition of a suitable form function $f_{L,G}(u)$ is required [Eqs. (11) and (16a)]. In the present work, the best-estimate shape is taken as input from the reference transport simulation, even if this is not possible in routine calculations. This allows us to keep the validation of the methodology unaffected by the inaccuracy unavoidably introduced adopting a leakage spectrum other than the exact one. It is thereby possible to focus on the effect of the chosen set of basis/weighting functions on the performance of the method. The development of a model for the leakage distribution is addressed in Sec. V.C.

The approximations of this rehomogenization approach (such as the lack of a spectral correction on the discontinuity factors) are discussed in Sec. V.A.1.

## III. MODAL SYNTHESIS OF THE SPECTRUM VARIATION

A paramount point in the definition of a modal-expansion method for the spectrum perturbation is the choice of a suitable set of basis and test functions. These

considerably affect the accuracy of the computed cross-section corrections.

Two kinds of basis functions have been investigated. The first approach adopts analytical functions (Chebyshev polynomials) in combination with a physically justified mode (the neutron emission spectrum from fission) in the fast group. The use of the latter is justified by the peak observed in the spectrum deformation at high energies (see Fig. 1b). Moreover, the fission spectrum is an appropriate trial function because it is mostly insensitive to the environmental conditions. An attempt has been made to find other modes having physical insight into the nature of the sought solution. This feature is highly desirable as it commonly requires a reasonably low number of basis functions to reproduce the solution to a satisfactory accuracy.[22] The behavior of neutrons in the epithermal and thermal parts of the spectrum can be described by the $1/E$-type slowing-down distribution and the Maxwellian distribution characterizing thermal equilibrium with the moderator.[23] However, a superposition of these migration modes can be used to synthesize only the neutron spectrum, not a spectrum perturbation. For instance, as the neutron temperature defining the Maxwellian distribution changes when moving from the infinite medium to the real environment, the thermal-spectrum variation cannot be described by such a function. Because of the difficulty of finding physical modes other than the fission spectrum, an alternative strategy has been formulated building upon the POD. This choice is inspired by the search of basis functions capturing some "information" of the phenomenon under study (i.e., the spectral interactions in a reactor core).

The two approaches are presented in Secs. III.A and III.B.

## III.A. The Polynomial-Based Approach

### III.A.1. Thermal-Group Basis Functions

In the thermal group, Chebyshev polynomials of the first kind $[T_i(u)]$ have been selected. The following recursive formula for $T_i(u)$ holds:

$$\begin{aligned} T_0(u) &= 1\,, \\ T_1(u) &= u\,, \\ T_i(u) &= 2uT_{i-1}(u) - T_{i-2}(u), \quad i \geq 2\,. \end{aligned} \tag{18}$$

In the pseudolethargy domain introduced in Sec. II [Eq. (6)], the thermal-group spectrum variation has value of zero for $u < b$, with $b \approx 0.5$. Therefore, a modification of Eq. (18) must be introduced in order for the basis functions to have zero average value in the interval $[b,1]$ and to be null in the interval $[0,b)$. The polynomials are first shifted to have zero average between 0 and 1:

$$T_i'(u) = T_i(u) - \int_0^1 du T_i(u), \quad i \geq 1\,. \tag{19}$$

Then, they are rescaled by means of a unitary Heaviside function $H(u-b)$, vanishing for $u < b$. According to the microgroup structure adopted in this work, a value of 0.52167 is chosen for $b$ to match the boundary of one of the fine-energy groups $g$. After these changes, the thermal basis functions read as

$$Q_{2,i}(u) = T_i'(u')H(u-b), \quad i \geq 1\,, \tag{20}$$

where the shifted variable $u'$ is defined as

$$u' = \frac{u-b}{1-b}\,. \tag{21}$$

The first four basis functions computed with Eq. (20) are shown in Fig. 2. Apparently, the superposition of the Heaviside function introduces a discontinuity in the modes for $u = b$.

### III.A.2. Fast-Group Basis Functions

In the fast group, the first trial function is the already mentioned fission-spectrum migration mode $\chi(u)$. Several expressions can be found in the literature for the neutron fission-emission spectrum. In this work, we use the formulation reported in Lamarsh's textbook.[24] In the energy domain, this reads as

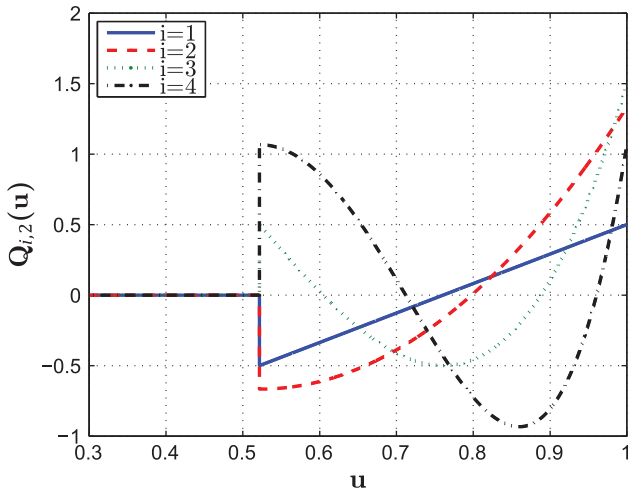


Fig. 2. Thermal-group polynomial basis functions.

$$\chi(E) = n_f \sqrt{E} e^{-a_f E} , \tag{22}$$

with $E$ expressed in mega-electron-volts (MeV). Equation (22) is derived under the assumption that the fission-emission distribution does not vary with the energy of the incident neutron. The coefficient $a_f$ and the normalization constant $n_f$ depend on the fissioning nuclides. We consider $a_f = 0.776$ and $n_f = 0.771$. These numerical values correspond to uranium fuel enriched at less than 10%. We assume that the inaccuracy caused by using Eq. (22) for other enrichments or different types of fuel material (such as MOX assemblies) is reasonably small and acceptable in the context of our application.

After moving from $E$ to $u$ and subtracting the average value of $\chi$, the basis function reads as

$$Q_{1,1}(u) = c e^{-a_f E_1^- r_1^u} \ln(r_1)(r_1^u)^{3/2} - \chi_{avg} , \tag{23}$$

where

$$\begin{aligned} \chi_{avg} &= \int_0^\infty dE \chi(E) = n_f \frac{\sqrt{\pi}}{2 a_f^{3/2}} , \\ c &= n_f (E_1^-)^{3/2} , \\ r_1 &= \frac{E_1^+}{E_1^-} . \end{aligned} \tag{24}$$

The remaining trial functions are, as in the thermal group, Chebyshev polynomials of the first kind (modified to have zero average value between 0 and 1):

$$Q_{1,i}(u) = T'_{i-1}(u), \quad i \geq 2 . \tag{25}$$

The fast-group basis functions are plotted in Fig. 3 for $i \in [1, 4]$.

### III.A.3. Weighting Functions

The achievement of satisfactory results with the above polynomial modes is strongly correlated to the test functions. Although their choice is in principle arbitrary, the weighting operators can be opted for to minimize the error in some sense.[22] For instance, the use of quasi-contiguous double step functions (i.e., 1 inside specified intervals and 0 outside) has the physical interpretation of requiring that the neutron balance be satisfied in an integral sense over certain regions of the energy domain. However, the importance of the various energy intervals can be sensitive to the specific configuration and, hence, lack generality. As finding a rigorous justification to the choice of the steps was not possible, this option has been discarded.

An attempt has been made to use the adjoint spectrum and the generalized importance functions computed at the lattice-calculation level. The physical meaning of this approach is to minimize the error on some characteristic spectrum-dependent integral quantity. Typical observables are, in this sense, the multiplication factor, the spectral index, the breeding ratio, resonance integrals, the $^{235}$U and $^{238}$U absorption probabilities per fission-emitted neutron, and the $^{135}$Xe worth, but other functionals of the spectrum can be defined.[25] This approach could not be implemented as a final solution because it produced an ill-conditioned matrix of the rehomogenization problem. Moreover, the adjoint and importance-function spectra in the real environment can differ from the infinite-medium ones. Hence, their use as test functions might not be rigorous.

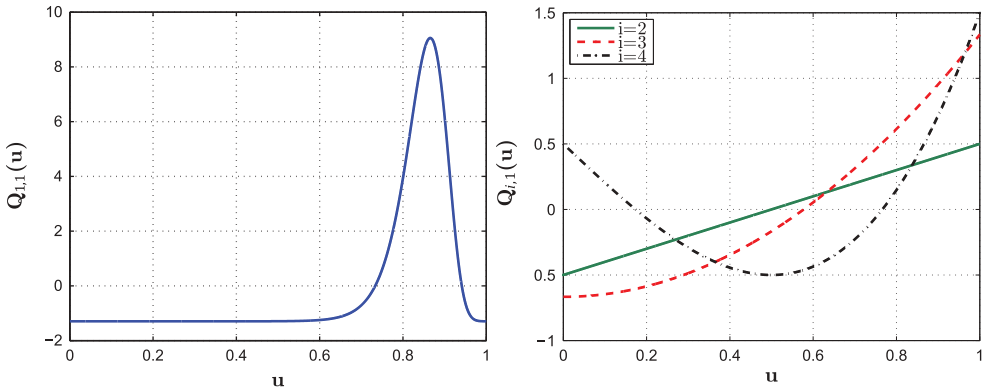


Fig. 3. Fast-group analytical basis functions: (a) neutron emission spectrum from fission and (b) Chebyshev polynomials of the first kind.

On the basis of these considerations, the most natural choice is to use Galerkin weighting (that is, using weighting functions equal to the basis functions).

### III.B. The POD Approach

The POD is a mathematical technique that has been widely used in the last decades in many scientific and engineering fields[26,27] and to which a growing interest has been recently shown also in the nuclear community.[28–32] In the context of our rehomogenization method, the proposed approach relies on the calculation of the optimal (in a least-squares sense) orthonormal basis functions for the space spanned by a set of snapshots of the reference spectrum variation (generally speaking, a snapshot is the solution of the equation modeling the problem of interest for a specific configuration or state of the system). The shape of these modes is determined by the energy (i.e., the information) carried within the retained snapshots and can thus capture some relevant features of the spectral changes. Even if the POD approach has a mathematical connotation (and not a physical one), its underpinning idea is to describe the spectrum variation as a modulation of functions synthesizing its main components. This is, to some extent, the same principle of the Migration Mode Method for the approximation of the neutron spectrum.[23]

As mentioned in Sec. I, interassembly heterogeneity is the main source of spectral effects, which mostly occur at the interface between different neighbor regions. Therefore, we simulate several assembly-interface types to generate snapshots of the spectrum variation between the environmental and infinite-medium conditions. We simplify our analysis by considering 2-D colorsets (i.e., four-assembly sets). The idea behind the generation of snapshots can be illustrated with an example. Figure 4 depicts the fast-group spectrum variation in a $UO_2$ assembly next to another $UO_2$ assembly with control rods inserted. Three different curves are shown as a function of the fuel enrichment in the rodded bundle (1.8%, 2.4%, 3.1%). The enrichment in the unrodded assembly is fixed (1.8%). Both assemblies have zero burnup.

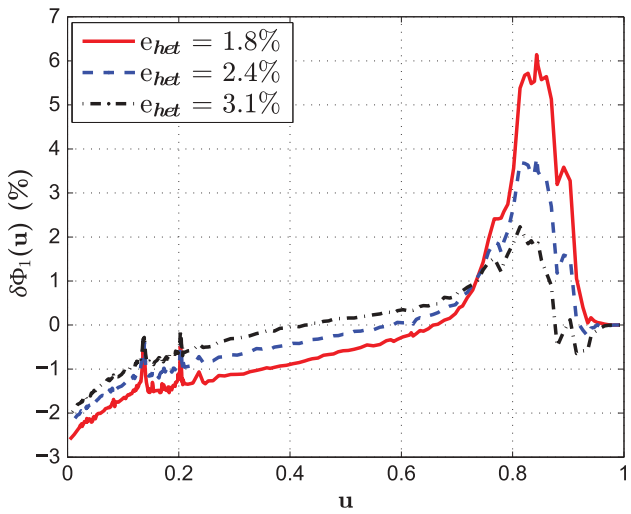


Fig. 4. Fast-group spectrum perturbation in a 1.8%-enriched $UO_2$ assembly as a function of the enrichment $e_{het}$ in the adjacent rodded $UO_2$ bundle.

In the epithermal range (that is, for approximately $u_1 < 0.6$), the curves exhibit a very much alike outline with roughly a simple shift among them. Also, a peak is found at high energies in the three cases. However, as long as the enrichment in the rodded assembly increases, a distortion of such peak occurs, with a sign-changing bulge becoming apparent. This suggests that interassembly heterogeneity in the enrichment triggers a characteristic component of the spectrum variation. The spectral interactions between adjacent assemblies can be driven by differences in a broad range of parameters other than the enrichment, such as the fuel composition and burnup, and by the presence of burnable poison and control elements. In order to cover the parameter space of spectral interfaces and to capture as many components of the spectrum variation as possible, multiple values of these heterogeneity variables must be sampled.

For a given configuration (corresponding to a certain set of the aforementioned parameters), we generate a snapshot by solving the neutron transport equation for the colorset and single-assembly configurations. The environmental and infinite-medium spatially averaged spectra are computed for each fuel bundle, together with the corresponding variation. In order to determine the detailed spectrum change, the numbers of fine-energy groups $g$ used in the fast and thermal coarse groups are 247 and 34, respectively. For both macrogroups, the matrix of snapshots $A_G$ is obtained collecting the spectrum variation solutions determined for different problems. The searched POD modes ensue from the Singular Value Decomposition (SVD) of $A_G$ (Ref. 32). This returns the following matrix decomposition:

$$A_G = U_G S_G V_G^T \ , \tag{26}$$

where $S_G$ is a diagonal matrix of size $n_G \times N_s$ ($n_G$ is the number of fine groups for the coarse group $G$ and $N_s$ is the number of snapshots), whereas $U_G$ and $V_G$ have dimensions $n_G \times n_G$ and $N_s \times N_s$, respectively. The columns of the matrix $U_G$ are referred to as proper orthonormal modes, and they are the sought POD basis. The elements of $S_G$, which are nonnegative and sorted in descending order, are the singular values of $A_G$. They are proportional to the energy of each mode, that is, its importance in the modal approximation of the vector space spanned by $A_G$. If all $n_G$

eigenvectors produced by the SVD are used, the error in the approximation of the original snapshot data goes to 0. The POD basis set for our rehomogenization method, consisting of $N_{Q_G}$ modes, is built from a reduced form of Eq. (26), taking the first $N_{Q_G}$ columns of $U_G$. The corresponding array provides a modal approximation of the snapshot set, which minimizes the error in the $L_2$-norm compared to all the other approximations. The rehomogenization problem is applied using the achieved POD modes also as weighting functions (Galerkin weighting).

### III.C. Integration in the LWR Two-Step Procedure

Figure 5 shows how the rehomogenization method is integrated in the nodal core calculation and, more in general, in the two-step procedure commonly adopted in LWR analysis.

The rehomogenization coefficients are computed [via Eq. (16)] at the cross-section library level by postprocessing the results of the fine-group transport simulation. Their calculation merely requires the solution of further integrals in the energy domain. The only change in the parameterized tables is the storage of the additional homogenization parameters. If the POD approach is used for the modal synthesis of the spectrum perturbations, a supplementary step is needed. Snapshots of the spectrum deformation have to be collected for various sample assembly configurations. They are then used to extract, via the SVD, the set of POD basis vectors with which the rehomogenization parameters are to be computed during the cross-section library preparation. The POD-basis calculation (to which we refer as "off-line" phase) is to be performed prior to the lattice calculation.

During the core calculation, a steady-state flux iteration of the nodal eigenvalue problem is first performed using the infinite-medium cross sections interpolated from the libraries at the current values of the state parameters in the various nodes. At the end of the nonlinear iteration, the nodal information ($\bar{\Phi}_G$, $\bar{L}_G$, $k_{eff}$) is used to solve the spectral rehomogenization problem. As this is done locally, sweeping the nodes of the system, the algorithm is easily parallelizable. Depending on the coupled neutronics/thermal-hydraulic iteration control criterion, the following may be stated:

1. If no thermal-feedback calculation is performed after the nodal-flux iteration, the single-assembly cross sections are updated with the spectral correction computed by rehomogenization.

2. If the thermal-feedback update is activated, the thermal-hydraulic calculation is performed using as input the nodal power $\bar{P}_G$ distribution from the prior flux iteration; after interpolation from the parameterized tables at the new values of the state parameters, the cross sections are updated with the spectral correction previously computed by rehomogenization.

Alternatively, the rehomogenization update can be implemented at an intermediate step between the nodal-flux and the thermal-feedback iterations. The calculation continues until convergence of all the coupled fields. Note that the flux solver is not changed by the rehomogenization module. Therefore, the method can be easily integrated in already existing core simulators.

## IV. VALIDATION

In this section the results of the spectral rehomogenization method are presented for some benchmark problems.

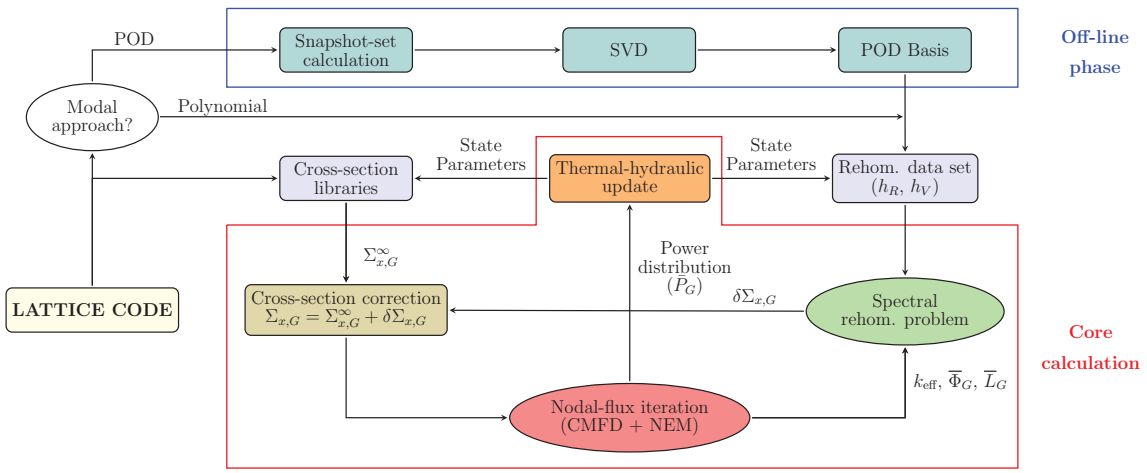


Fig. 5. Flow diagram of spectral rehomogenization within the LWR two-step calculation.

Both POD-based and polynomial-based approaches are considered. The analysis of the results is introduced by a description of the procedure followed for the validation.

## IV.A. Procedure

We apply spectral rehomogenization to three test cases exhibiting significant heterogeneity: a $UO_2$ colorset with burnable poison rods (example 1), a $UO_2$ colorset hosting silver-indium-cadmium (AIC) control rods (example 2), and a $UO_2$/MOX colorset (example 3). The nodal calculations are performed with BRISINGR, a Delft University of Technology in-house–developed code based on a standard nonlinear Coarse Mesh Finite Difference (CMFD) – Nodal Expansion Method (NEM) solution strategy. The two-group homogenization parameters are computed by the SERPENT continuous-energy Monte Carlo neutron transport code.[33] Version 2.1.28 of SERPENT is used in combination with the JEFF3.1 nuclear data library.[34]

The single-assembly calculations for group-constant generation are run with 750 active cycles of $7.5 \times 10^5$ source neutrons (50 inactive cycles are discarded to allow the initial fission-source distribution to converge). This choice results in $5.63 \times 10^8$ active neutron histories. A standard deviation lower than 2.5% has been found for all the input cross sections and discontinuity factors. Therefore, an uncertainty-propagation analysis is deemed not to be necessary for the scope of this work. No critical-buckling correction is applied to the two-group cross sections (as clarified later, this choice is consistent with the calculation of the snapshots in the POD-approach framework). We use two-group diffusion coefficients computed with the Cumulative Migration Method[35] (CMM). The simulations are made for initial-core isothermal conditions (i.e., without thermal hydraulics and fuel depletion feedbacks). The values of the main state parameters correspond to standard hot-full-power conditions (namely, $T_{fuel}$ = 846 K, $T_{mod}$ = 582 K, $p$ = 158 bar). We adopt a nodalization of $2 \times 2$ nodes per assembly.

The nodal calculations are compared to the reference solution from SERPENT. In this work, we address only the errors in the node-averaged quantities. For each benchmark problem, the results of four types of simulation are shown: (a) with standard infinite-medium cross sections from the parameterized libraries, (b) with cross sections corrected by means of the reference spectral defect, (c) with polynomial-based spectral rehomogenization of cross sections, and (d) with POD-based spectral rehomogenization of cross sections. For both modal approaches, rehomogenization is applied with $N_{Q_G} = 4$ in each coarse group. The reference spectral defect is evaluated, in line with Eq. (17), by collapsing the fine-group cross-section distribution $\Sigma^{\infty}_{x,G}(u)$ with the reference spectrum variation $\delta\Phi^{ref}_G(u)$ computed in SERPENT:

$$\delta\Sigma^{ref,spectr}_{x,G} = \frac{1}{\bar{\Phi}_G}\int_0^1 du \Sigma^{\infty}_{x,G}(u)\delta\Phi^{ref}_G(u)\,. \tag{27}$$

This choice is made because of the double nature (spatial and spectral) of the homogenization error. Since only the spectral error is addressed here, the homogenization defect cannot be fully corrected. In the analysis, the errors in the nodal cross sections are computed as

$$\Delta\Sigma_{x,G} = \frac{\Sigma_{x,G} - \Sigma^{ref}_{x,G}}{\Sigma^{ref}_{x,G}} \cdot 100\%\,, \tag{28}$$

where $\Sigma_{x,G}$ is the infinite-medium or rehomogenized cross section and $\Sigma^{ref}_{x,G}$ is the reference cross section (i.e., homogenized in the colorset environment).

The snapshots for the calculation of the POD modes are computed with SERPENT as well. Each 281-group spectrum variation solution is obtained running $5.25 \times 10^6$ active neutron histories. This value is a reasonably good compromise between statistical accuracy and computational effort. For reasons related to the computing time, the $B_1$ critical-spectrum calculation is not performed for the fine-group flux distributions. More details about the procedure for the generation of snapshots are given for each test case in Sec. IV.B.

## IV.B. Numerical Results

### IV.B.1. Example 1: $UO_2$ Colorset with Pyrex Rods

The 2-D colorset is depicted in Fig. 6. It consists of four $17 \times 17$ PWR fuel assemblies of fresh $UO_2$ having two different compositions: the former with 1.8% enrichment, the latter with 3.1% enrichment and 16 rods containing burnable absorber (Pyrex). The concentration of diluted boron in the moderator is 700 parts per million (ppm).

In this configuration, the interassembly spectral effects are driven by the different enrichments and by the local presence of burnable poison elements. In order to calculate a set of POD modes, we generate 100 snapshots by means of a single-parameter analysis, with the content of borosilicate glass in the heterogeneous assembly (namely, the assembly with poison rods) as

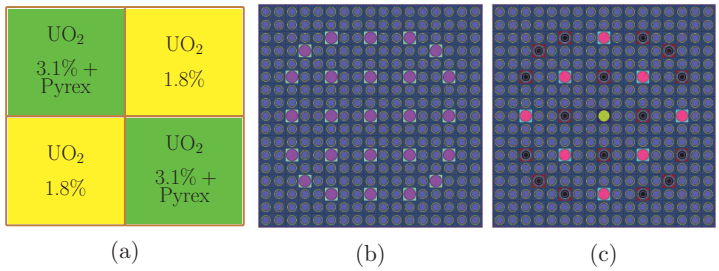


Fig. 6. (a) Assembly set and layout of the $UO_2$ fuel assemblies with (b) 1.8% enrichment and (c) 3.1% enrichment and Pyrex rods. The two bundles host 25 and 9 Zircaloy-4 guide tubes, respectively.

the parametric variable. Solutions of the spectrum variation are computed sampling uniformly the target range $[5.9 \times 10^{-5}, 1.8 \times 10^{-3}]$ atoms/cm$^3$ for the concentration of boron in the burnable-absorber rods $N^{bp}_{B_{10}}$. The snapshots are taken at a diluted-boron concentration of 1465 ppm. In the nodal calculation we simulate the colorset for one of the values of $N^{bp}_{B_{10}}$ spanned by the snapshot matrix (i.e., $9.3 \times 10^{-4}$ atoms/cm$^3$). This is done in order to test the capability of the POD modes to accurately reproduce the solutions used to build the original snapshot set. The chosen absorber concentration corresponds to $k_{eff}$ = 1.08733 (reference value).

Figure 7 shows the best-fit curves of the reference spectrum variation in the heterogeneous assembly. These have been computed with the polynomial basis functions and with the first four POD modes generated by the above procedure. The latter are plotted in Fig. 8. The POD operators fit very well the reference curves.

By comparing Figs. 7 and 8, it is apparent that the first- and second-order POD basis retrieve the global shape of the reference spectrum perturbation. The spiky profiles observable in the higher-order modes, especially in the epithermal region, contribute to the reconstruction of the fine details of $\delta\Phi(u)$, including those associated with the resonances. Obviously, the Chebyshev polynomials cannot reproduce such fine details due to their smoothness. However, they fit the average behavior of the reference curves precisely. The POD modes inherit the property of the $\delta\Phi$ snapshots to have zero average within each macrogroup.

The spectrum change estimated by rehomogenization with the two modal strategies is plotted in Fig. 9. The polynomial approach accurately predicts the perturbation in the epithermal region, whereas the reconstruction of the high-energy peak is less precise. In the thermal group, the computed curve is "tilted" with respect to the reference one due to the discontinuity in the analytical definition of the modified Chebyshev polynomials. With the

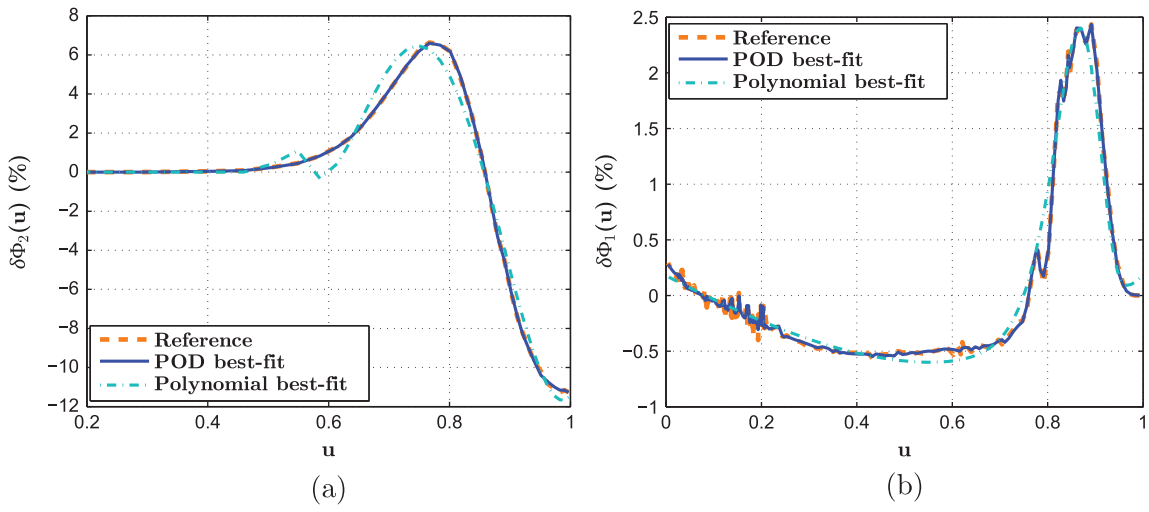


Fig. 7. Example 1: Best fit of the (a) thermal-group and (b) fast-group reference spectrum deformation (per unit $u$) for the assembly hosting burnable absorber rods. The perturbation is computed with respect to the assembly-averaged fluxes $\bar{\Phi}_G$ from the reference transport calculation.

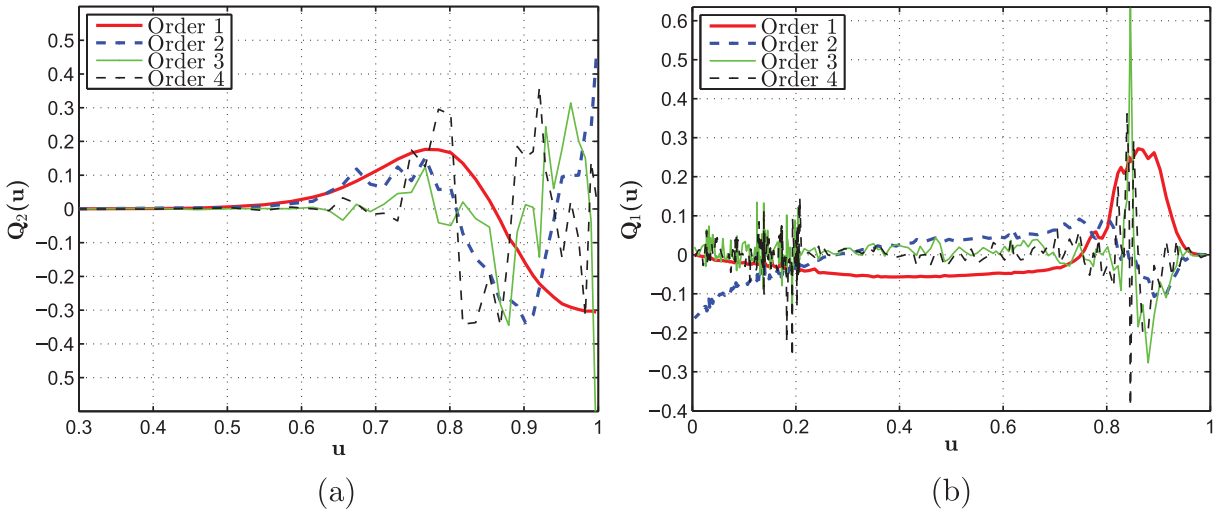


Fig. 8. (a) Thermal-group and (b) fast-group POD basis functions computed via the method of snapshots and SVD for a one-parameter analysis of example 1.

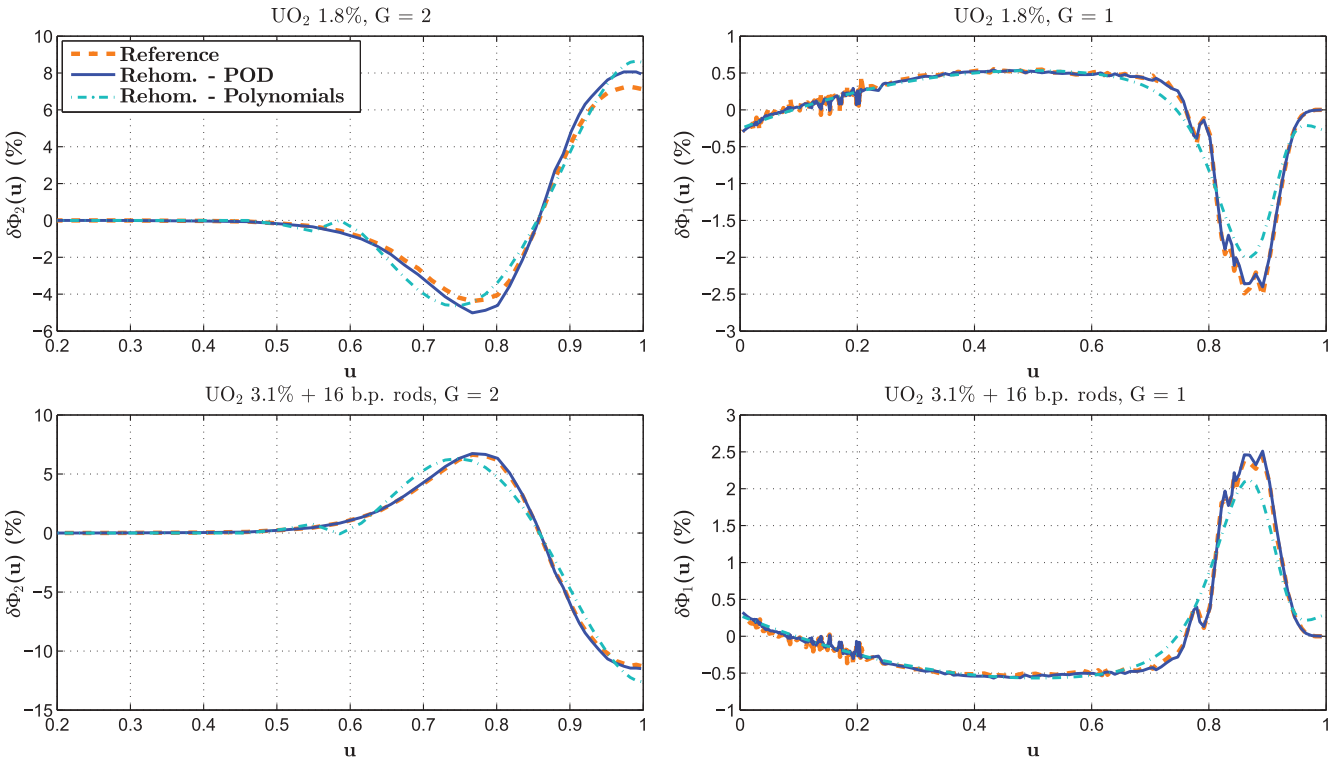


Fig. 9. Example 1: Spectrum variation per unit $u$ computed by rehomogenization.

POD method, the reconstruction is excellent in the fast group. The prediction in the thermal group is also very accurate in the assembly with burnable absorber, whereas a slight overestimation of the reference-curve magnitude is observed in the homogeneous assembly (i.e., the assembly without poison rods).

Table I reports the results in terms of $k_{eff}$ and assembly average power $P_{avg}$ for nodal calculations *a, b, c*, and *d*. The number of power iterations for the convergence of the eigenvalue problem is also given. The power errors within parentheses correspond to the fast (first value) and thermal (second value) groups. The effectiveness of rehomogenization in improving the nodal fission power is apparent, while the gain in accuracy in the multiplication factor is somewhat limited. This is caused by the fact that the effects of spatial changes in the flux distribution are not

TABLE I

Example 1: Errors in the Multiplication Factor and Nodal Fission Power

| Simulation | Number of Power Iterations | $\Delta k_{eff}$ (pcm) | $UO_2$ 1.8% | $UO_2$ 3.1% + 16 Burnable Poison Rods |
|---|---|---|---|---|
| | | | Error on $P_{avg}$ (%) | Error on $P_{avg}$ (%) |
| Standard (*a*) | 8 | −403 | 0.55 (0.68, 0.53) | −0.48 (−0.49, −0.49) |
| Reference $\delta\Sigma^{spectr}$ (*b*) | 8 | −373 | 0.03 (0.37, −0.04) | −0.02 (−0.26, 0.04) |
| Spectral rehomogenization Chebyshev (*c*) | 15 | −369 | −0.02 (0.37, −0.09) | 0.01 (−0.26, 0.09) |
| Spectral rehomogenization POD (*d*) | 22 | −369 | −0.01 (0.36, −0.09) | 0.01 (−0.26, 0.08) |

accounted for by the present method. Tables II and III show the errors in the nodal cross sections for the two assemblies. For both approaches, the cross-section corrections computed by rehomogenization reproduce almost exactly the reference ones (calculation *b*). No significant difference is found between the two sets of basis functions despite the higher accuracy of the POD approach emerging from Fig. 9, especially within the thermal group.

As seen in Table I, the rehomogenization method causes an increase in the number of nonlinear iterations by a factor of 1.9 when Chebyshev polynomials are used and by a factor of 2.8 when the POD modes are adopted. The number of power iterations reported in Table I corresponds to a tolerance of $10^{-5}$ for the relative variation of the $k_{eff}$ estimate and of the nodal-flux distribution 2-norm.

An analysis is now carried out on the impact of the diffusion-coefficient spectral correction $\delta D_G$. The diffusion coefficient can be rehomogenized in a similar fashion to the other cross sections by defining its zeroth-order variational coefficient:

$$h_{V,D,G,i,0} = \int_0^1 du D_G^{\infty}(u) Q_{G,i}(u) \,. \tag{29}$$

Hence, the following relation holds for $\delta D_G$:

$$\delta D_G = \frac{1}{\bar{\Phi}_G} \sum_{i=1}^{N_{Q_G}} \alpha_{G,i} h_{V,D,G,i,0} \,. \tag{30}$$

We consider as example the calculation with the reference spectral corrections (calculation *b*). In the version of SERPENT used in this work, the CMM can be only applied when the homogenized region covers the entire geometry. Therefore, the simulation is repeated with the outflow transport approximation[36] for the calculation of the diffusion coefficients (in this way, a comparison between the environmental and infinite-medium values is possible). For this option, Table IV reports the main results of the simulations with (*e*) the reference corrections on the cross sections and (*f*) the reference

TABLE II

Example 1: Errors in the Nodal Cross Sections of the Assembly Without Pyrex Rods

| $UO_2$ 1.8% | $\Sigma_{a,1}$ | $\Sigma_{a,2}$ | $\nu\Sigma_{f,1}$ | $\nu\Sigma_{f,2}$ | $\Sigma_{t,1}$ | $\Sigma_{t,2}$ | $\Sigma_{s,1\to1}$ | $\Sigma_{s,1\to2}$ | $\Sigma_{s,2\to2}$ |
|---|---|---|---|---|---|---|---|---|---|
| Reference ($cm^{-1}$) | 0.00877 | 0.0690 | 0.00485 | 0.0815 | 0.539 | 1.309 | 0.513 | 0.0178 | 1.238 |
| Simulation | Error (%) | | | | | | | | |
| Standard (*a*) | −0.25 | 0.73 | 0.40 | 0.82 | −0.25 | 0.27 | −0.27 | 0.13 | 0.25 |
| Reference $\delta\Sigma^{spectr}$ (*b*) | 0.04 | 0.17 | 0.14 | 0.24 | 0.0 | −0.05 | 0.0 | −0.03 | −0.06 |
| Spectral rehomogenization Chebyshev (*c*) | 0.06 | 0.11 | 0.15 | 0.17 | −0.01 | −0.07 | −0.01 | −0.04 | −0.08 |
| Spectral rehomogenization POD (*d*) | 0.0 | 0.10 | 0.14 | 0.17 | 0.0 | −0.08 | 0.0 | −0.05 | −0.09 |

TABLE III

Example 1: Errors in the Nodal Cross Sections of the Assembly with Pyrex Rods

| $UO_2$ 3.1% + 16 Burnable Poison Rods | $\Sigma_{a,1}$ | $\Sigma_{a,2}$ | $\nu\Sigma_{f,1}$ | $\nu\Sigma_{f,2}$ | $\Sigma_{t,1}$ | $\Sigma_{t,2}$ | $\Sigma_{s,1\to1}$ | $\Sigma_{s,1\to2}$ | $\Sigma_{s,2\to2}$ |
|---|---|---|---|---|---|---|---|---|---|
| Reference ($cm^{-1}$) | 0.0101 | 0.1040 | 0.00659 | 0.132 | 0.525 | 1.296 | 0.499 | 0.016 | 1.190 |
| Simulation | Error (%) | | | | | | | | |
| Standard (*a*) | 0.27 | −0.49 | −0.22 | −1.11 | 0.26 | −0.49 | 0.27 | −0.17 | −0.50 |
| Reference $\delta\Sigma^{spectr}$ (*b*) | −0.02 | 0.33 | −0.11 | −0.21 | 0.0 | 0.0 | 0.0 | 0.0 | −0.02 |
| Spectral rehomogenization Chebyshev (*c*) | −0.03 | 0.33 | −0.10 | −0.21 | 0.0 | 0.0 | 0.0 | 0.05 | −0.02 |
| Spectral rehomogenization POD (*d*) | 0.01 | 0.34 | −0.09 | −0.20 | 0.0 | 0.02 | 0.0 | 0.06 | 0.0 |

corrections on the cross sections and diffusion coefficients. In calculation *f* the correction $\delta D_G$ is also computed with the reference spectrum change. The errors $\Delta$ in the nodal power and diffusion coefficients are expressed in percentage.

Rehomogenization with the reference spectrum variation nullifies the errors in $D_G$. However, the diffusion-coefficient corrections have clearly no impact on the integral parameters. This is because the corrections $\delta D_G$ are not large enough to bring about appreciable changes in the neutron flux distribution. Such consideration can be justified as follows. If Table I (calculation *b*) and Table IV (calculation *e*) are compared, it appears that the outflow transport approximation produces a significant variation of the error in the thermal power with respect to the CMM. As the other input parameters of the nodal calculation are unchanged, this variation is only caused by the differences between the values of $D_G$ computed with the two definitions, which are quite large. For instance, in the assembly with Pyrex rods the fast-group diffusion coefficient from the outflow transport approximation is 6.2% higher than the one from the CMM, whereas the thermal-group value is nearly 10% lower. On the other hand, the corrections $\delta D_G$ computed by rehomogenization are much smaller: −0.33% ($G = 1$) and 0.51% ($G = 2$) in the homogeneous assembly; 0.33% ($G = 1$) and −0.73% ($G = 2$) in the heterogeneous one. Thus, the errors in the integral parameters are unaffected. This feature has been systematically observed also for the other benchmark problems. It can be concluded that the diffusion-coefficient rehomogenization does not bring any substantial benefit to the accuracy of the nodal calculation.

### IV.B.2. Example 2: $UO_2$ Colorset with AIC Control Rods

The colorset is made of four $17 \times 17$ $UO_2$ bundles with 1.8% enrichment (Fig. 10). Two assemblies host 24 AIC control rods. No boron is present in the moderator ($C_{B_{10}} = 0$ ppm). The reference multiplication factor is 0.98860.

In order to build a set of snapshots representative of the spectral effects induced by control elements and different enrichments, we parameterize the system using three variables:

1. the fuel enrichment, which is homogeneously sampled in the interval [2.1%, 3.6%] for both

TABLE IV

Example 1: Impact of Diffusion-Coefficient Rehomogenization

| Simulation | $\Delta k_{eff}$ (pcm) | $UO_2$ 1.8% | | | $UO_2$ 3.1% + 16 Burnable Poison Rods | | |
|---|---|---|---|---|---|---|---|
| | | $\Delta P_{avg}$ | $\Delta D_1$ | $\Delta D_2$ | $\Delta P_{avg}$ | $\Delta D_1$ | $\Delta D_2$ |
| Reference $\delta\Sigma^{spectr}$ (*e*) | −376 | 0.42 (0.52, 0.40) | 0.29 | −0.48 | −0.37 (−0.37, −0.37) | −0.28 | 0.72 |
| Reference $\delta\Sigma^{spectr}$ and $\delta D_G$ (*f*) | −376 | 0.42 (0.52, 0.41) | −0.05 | 0.03 | −0.37 (−0.37, −0.37) | 0.05 | −0.02 |

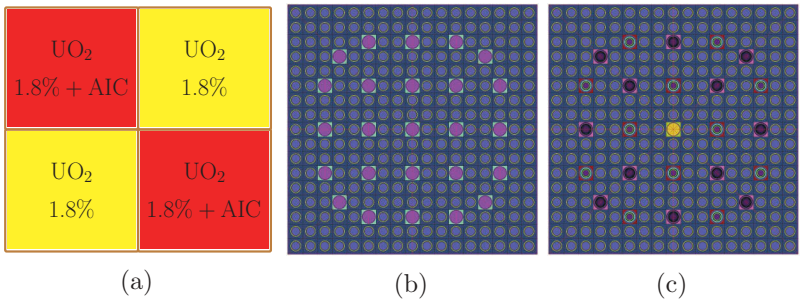


Fig. 10. (a) Assembly set and layout of the (b) unrodded and (c) rodded $UO_2$ fuel assemblies with 1.8% enrichment. The bundle without control rods hosts 25 empty guide tubes.

the rodded and unrodded assemblies (20 combinations are selected)

2. the number of control rods inserted in each heterogeneous fuel bundle (4, 8, 12, 16, 24, 28), changed keeping the symmetry in the assembly layout
3. the types of control rods (AIC and $B_4C$).

A total number of 240 snapshots are computed. In order to verify whether the POD approach can accurately predict the spectrum deformation for unseen problems (i.e., problems whose solution was not included in the snapshot array), rehomogenization is applied to the present colorset also with the set of modes determined for example 1. In the analysis, we refer to the nodal simulations with the POD modes of examples 1 and 2 as $d1$ and $d2$, respectively.

The spectrum deformation computed by rehomogenization is reported in Fig. 11. The set of POD basis functions from the multiparameter analysis perfectly reconstructs the fast-group deformation. A very accurate outcome is also found with the set of modes derived for the colorset with Pyrex rods, even if a slight distortion of the computed distributions arises within the fast group in proximity of the high-energy peak. In the thermal group,

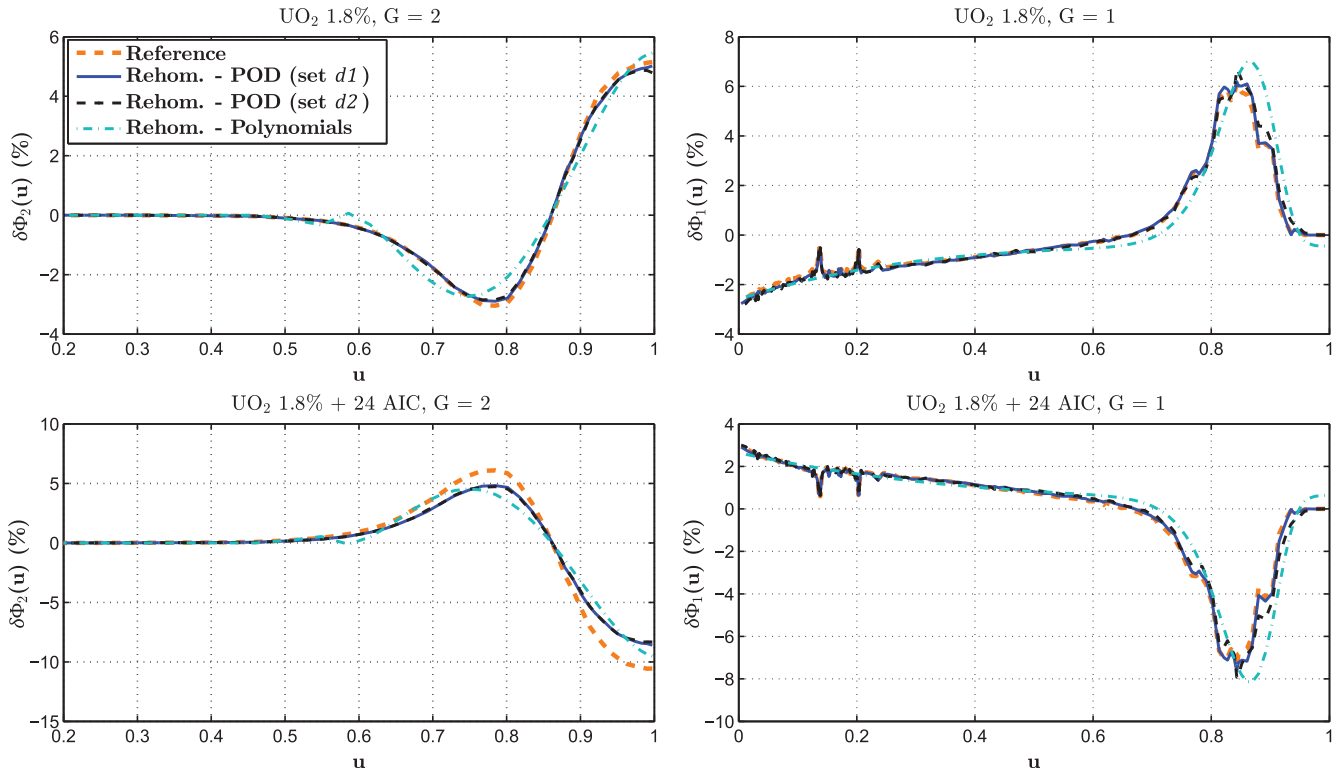


Fig. 11. Example 2: Spectrum variation per unit $u$ computed by rehomogenization.

no appreciable difference is encountered between the two calculations. In both of them, the magnitude of the spectrum variation is underestimated in the higher part of the thermal domain ($u_2 \in [0.85,1.0]$) and in its intermediate region ($u_2 \in [0.6,0.85]$), especially in the assembly with control rods. With the polynomial approach, in the fast group the computed high-energy peak is shifted toward higher values of $u$ with respect to the reference curve. In the thermal group, similar considerations hold as for the POD basis functions.

The inaccuracy observed in the predicted thermal-spectrum perturbation can be explained as follows. For the rodded assembly, the relative correction $\delta\Sigma_{a,2}^{ref,spectr}$ is 0.59%. However, the global variation $\delta\Sigma_{a,2}^{ref,tot}$ (that is, the relative difference between the cross sections homogenized in the colorset environment and in the single-assembly configuration) is −0.71%. This means that the spatial correction must go in the opposite direction of the spectral one and that it constitutes a significant part of the homogenization defect (under the hypothesis of full superimposition of the two corrections, it would correspond to a relative change $\delta\Sigma_{a,2}^{ref,spat} \approx -1.31\%$). Since the thermalizing effect of the spatial term is not taken into account here, the method predicts a harder spectrum (that is, it underestimates $\delta\Phi_2$ as previously highlighted). In the unrodded assembly, $\delta\Sigma_{a,2}^{ref,spectr}$ is −0.37%, whereas the global variation $\delta\Sigma_{a,2}^{ref,tot}$ is −0.56%. Hence, the spatial correction must be $\delta\Sigma_{a,2}^{ref,spat} \approx -0.19\%$. As in this case the mismatch between the two corrections is smaller, the differences between the simulated and reference curves are less evident.

The errors in the integral parameters and nodal cross sections are reported in Tables V, VI, and VII. The unexpectedly small error on $k_{eff}$ in the standard

TABLE V

Example 2: Errors in the Multiplication Factor and Nodal Fission Power

| Simulation | Number of Power Iterations | $\Delta k_{eff}$ (pcm) | $UO_2$ 1.8% | $UO_2$ 1.8% + 24 AIC Rods |
|---|---|---|---|---|
| | | | Error on $P_{avg}$ (%) | Error on $P_{avg}$ (%) |
| Standard (*a*) | 10 | 58 | 3.03 (0.98, 3.41) | −4.70 (−1.17, −5.61) |
| Reference $\delta\Sigma^{spectr}$ (*b*) | 10 | −486 | 1.14 (0.47, 1.28) | −1.77 (−0.56, −2.10) |
| Spectral rehomogenization Chebyshev (*c*) | 17 | −513 | 1.25 (0.73, 1.36) | −1.94 (−0.87, −2.24) |
| Spectral rehomogenization POD (*d*1) | 25 | −543 | 1.14 (0.60, 1.25) | −1.77 (−0.71, −2.06) |
| Spectral rehomogenization POD (*d*2) | 20 | −524 | 1.16 (0.50, 1.29) | −1.80 (−0.60, −2.13) |

TABLE VI

Example 2: Errors in the Nodal Cross Sections of the Unrodded Assembly

| $UO_2$ 1.8% | $\Sigma_{a,1}$ | $\Sigma_{a,2}$ | $\nu\Sigma_{f,1}$ | $\nu\Sigma_{f,2}$ | $\Sigma_{t,1}$ | $\Sigma_{t,2}$ | $\Sigma_{s,1\to1}$ | $\Sigma_{s,1\to2}$ | $\Sigma_{s,2\to2}$ |
|---|---|---|---|---|---|---|---|---|---|
| Reference ($cm^{-1}$) | 0.00827 | 0.0557 | 0.00485 | 0.0837 | 0.534 | 1.313 | 0.509 | 0.0174 | 1.256 |
| Simulation | Error (%) | | | | | | | | |
| Standard (*a*) | 1.61 | 0.56 | 0.51 | 0.60 | 0.68 | 0.16 | 0.56 | 3.80 | 0.14 |
| Reference $\delta\Sigma^{spectr}$ (*b*) | 0.05 | 0.20 | −0.12 | 0.23 | −0.02 | −0.05 | −0.02 | −0.07 | −0.06 |
| Spectral rehomogenization Chebyshev (*c*) | −0.53 | 0.21 | 0.05 | 0.24 | −0.14 | −0.04 | −0.13 | −0.23 | −0.05 |
| Spectral rehomogenization POD (*d*1) | −0.08 | 0.21 | −0.07 | 0.24 | −0.08 | −0.04 | −0.07 | −0.38 | −0.05 |
| Spectral rehomogenization POD (*d*2) | −0.04 | 0.20 | −0.14 | 0.24 | −0.06 | −0.04 | −0.05 | −0.29 | −0.06 |

TABLE VII

Example 2: Errors in the Nodal Cross Sections of the Rodded Assembly

| $UO_2$ 1.8% + 24 AIC rods | $\Sigma_{a,1}$ | $\Sigma_{a,2}$ | $\nu\Sigma_{f,1}$ | $\nu\Sigma_{f,2}$ | $\Sigma_{t,1}$ | $\Sigma_{t,2}$ | $\Sigma_{s,1\rightarrow1}$ | $\Sigma_{s,1\rightarrow2}$ | $\Sigma_{s,2\rightarrow2}$ |
|---|---|---|---|---|---|---|---|---|---|
| Reference ($cm^{-1}$) | 0.0116 | 0.0817 | 0.00474 | 0.0853 | 0.534 | 1.286 | 0.507 | 0.0153 | 1.203 |
| Simulation | Error (%) | | | | | | | | |
| Standard (*a*) | −1.71 | 0.71 | −0.64 | −0.93 | −0.80 | −0.38 | −0.66 | −4.77 | −0.46 |
| Reference $\delta\Sigma^{spectr}$ (*b*) | 0.60 | 1.28 | 0.19 | −0.12 | 0.02 | 0.05 | 0.0 | 0.01 | −0.04 |
| Spectral rehomogenization Chebyshev (*c*) | 1.02 | 1.15 | −0.09 | −0.30 | 0.13 | −0.05 | 0.12 | −0.17 | −0.14 |
| Spectral rehomogenization POD (*d*1) | 0.66 | 1.15 | 0.0 | −0.30 | 0.08 | −0.05 | 0.07 | 0.07 | −0.13 |
| Spectral rehomogenization POD (*d*2) | 0.58 | 1.15 | 0.10 | −0.30 | 0.04 | −0.05 | 0.03 | −0.06 | −0.13 |

calculation is the result of fortuitous error compensation as evidenced by the high deviations in the nodal power. This error cancellation vanishes when spectral rehomogenization is applied. The simulation with the reference corrections is well reproduced by the calculations with the rehomogenized cross sections. It still exhibits a somewhat high error in the multiplication factor and thermal power, which confirms the need of applying spatial rehomogenization to fully take into account the environmental effects. For instance, it has been found that when applying the POD-based spectral rehomogenization (calculation *d*2) to the cross sections rehomogenized with the reference spatial corrections, the error in $k_{eff}$ drops from −524 to −3 pcm.

When looking at the deviations in the nodal cross sections, the underestimation of the spectrum change in different regions of the thermal domain causes some beneficial error cancellation in thermal absorption in both assemblies as well as in thermal production $\nu\Sigma_{f,2}$ in the fuel bundle without control rods. Despite the inaccuracy in the calculation of the thermal-spectrum change, the corrections determined by rehomogenization are very close to the reference ones, apart from a slight overestimation of $\delta\nu\Sigma_{f,2}$ in the rodded assembly and of $\delta\Sigma_{s,1\rightarrow2}$ in the unrodded one. The fast-absorption correction is overestimated when Chebyshev polynomials are used. This is because the polynomial basis functions do not capture the resonance peaks in the epithermal region (for $u_1 \in [0.05, 0.25]$), where the computed spectrum variation underestimates (in magnitude) the reference curve. Since the fine-group absorption cross sections are considerably high in proximity of the resonance energies, an overestimated $\delta\Sigma_{a,1}$ is found in the rodded assembly (the opposite occurs in the unrodded one).

In this test case, the gap between the two modal approaches in terms of additional nonlinear iterations is much less substantial. As shown in Table V, the number of outer iterations increases by a factor of 1.7 when the polynomial basis is used and by a factor of 2 with the POD approach. In the framework of the POD analysis, the modes computed for example 1 (i.e., a colorset with burnable absorber rods) can approximate the spectrum perturbation with an accuracy comparable to those computed ad hoc for rodded configurations. This is because spectral interactions in the two example problems share common features.

### *IV.B.3. Example 3: $UO_2$/MOX Colorset*

The third colorset, which is shown in Fig. 12, consists of two 18 × 18 $UO_2$ and MOX assemblies. The $UO_2$ assembly has enrichment of 2.1%. Three different fuel pin types are present in the MOX assembly: with low Pu content (1.78% $^{239}$Pu, 0.22% $^{235}$U) at the assembly corners, with intermediate Pu content (2.53% $^{239}$Pu, 0.21% $^{235}$U) along the assembly outer edges, and with high Pu content (3.86% $^{239}$Pu, 0.20% $^{235}$U) in the remainder of the fuel bundle. The concentration of soluble boron in the moderator is 2907 ppm. The reference multiplication factor is 1.00194.

The polynomial-based rehomogenization is applied with four (calculation *c*1) and seven (calculation *c*2) modes in the fast group. In the latter case, the fission spectrum and the Chebyshev functions of orders 1 through 6 are used. The POD-based rehomogenization is applied making use of three sets of basis functions:

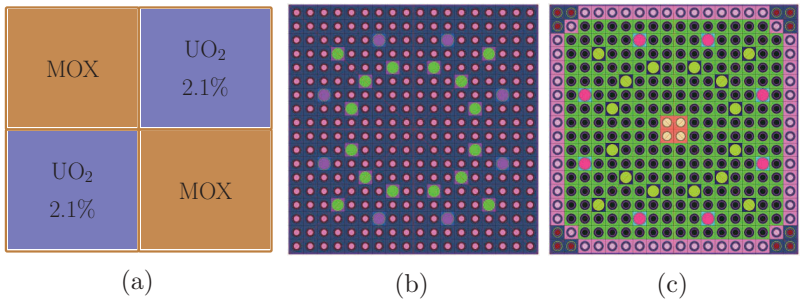


Fig. 12. (a) Assembly set and layout of the (b) $UO_2$ and (c) MOX fuel assemblies. The MOX assembly is made of three fuel pin types differing for their Pu content and U enrichment.

1. the POD modes computed for example 1 (set *d*1)
2. the POD modes obtained from a multiparameter study for the present configuration (set *d*2)
3. the POD modes obtained assembling all the snapshots computed for the three benchmark problems investigated in this work (set *d*3).

We refer to the nodal simulations with these three sets of basis functions as *d*1, *d*2, and *d*3, respectively. The generation of snapshots for the $UO_2$-MOX interface is performed following the example of test cases 1 and 2, namely, considering the $UO_2$ enrichment and the Pu content in the three MOX assembly pin types as parametric variables. The purpose of calculation *d*3 is to verify whether rehomogenization, applied with few modes, can still synthesize effectively the spectral deformations associated with various assembly-interface types, exhibiting a considerably unlike behavior of δΦ (especially in the fast range). This property of the POD modes is essential for the feasibility of the methodology at an industrial level, in which the use of modes not depending on the type of fuel element would be highly desirable.

Figure 13 shows the $UO_2$ assembly fast-group spectrum variation calculated with the set of modes *d*1. In this case, rehomogenization has been applied with the basis functions resulting from the SVD of high-order Legendre polynomial best fits of the original snapshots. This strategy eliminates the noise caused by a different pattern of the spectrum change fine details in the two configurations, still preserving the global shape of the snapshots. Although the accuracy of the calculation is acceptable in the epithermal range, the method is not capable of recreating the bump observable at the end of the pseudolethargy domain (for $u_1 \in [0.87,1.0]$). This is expected, as the POD basis computed for the colorset with Pyrex rods has not been trained to reproduce such a localized, abruptly sign-changing feature. We already observed this particular shape in Fig. 4, when the effect of increasing enrichment on the δΦ distribution was shown for

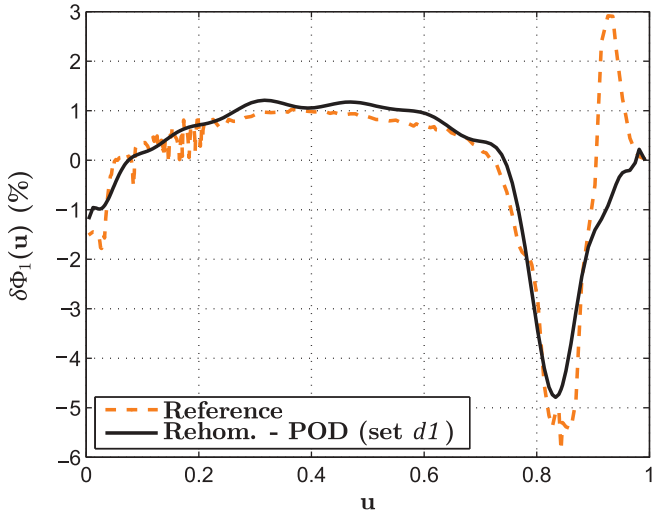


Fig. 13. Example 3: Fast-group spectrum variation in the $UO_2$ assembly computed with the POD modes derived for example 1.

an assembly set with control rods (also for a generic $UO_2$-MOX interface, it has been found that such component of the spectrum deformation becomes more pronounced when the enrichment in the $UO_2$ bundle is increased).

The spectrum variation computed with calculations *c*1, *c*2, and *d*3 is shown in Fig. 14. As results obtained with simulation *d*2 are almost identical to those of simulation *d*3, they are not reported for the sake of brevity. Rehomogenization with the set of modes *d*3 faithfully reproduces the bulge observed in the fast group. Such outcome can be achieved only by a proper training of the POD modes, that is, if solutions exhibiting this particular feature are included in the snapshot array. This can be deduced from Fig. 15a, showing the fast-group POD basis functions computed from the snapshot set *d*3. Apparently, the shape of the high-energy bulge is retained by the second-, third-, and fourth-order modes. The second mode also inherits the steep profile

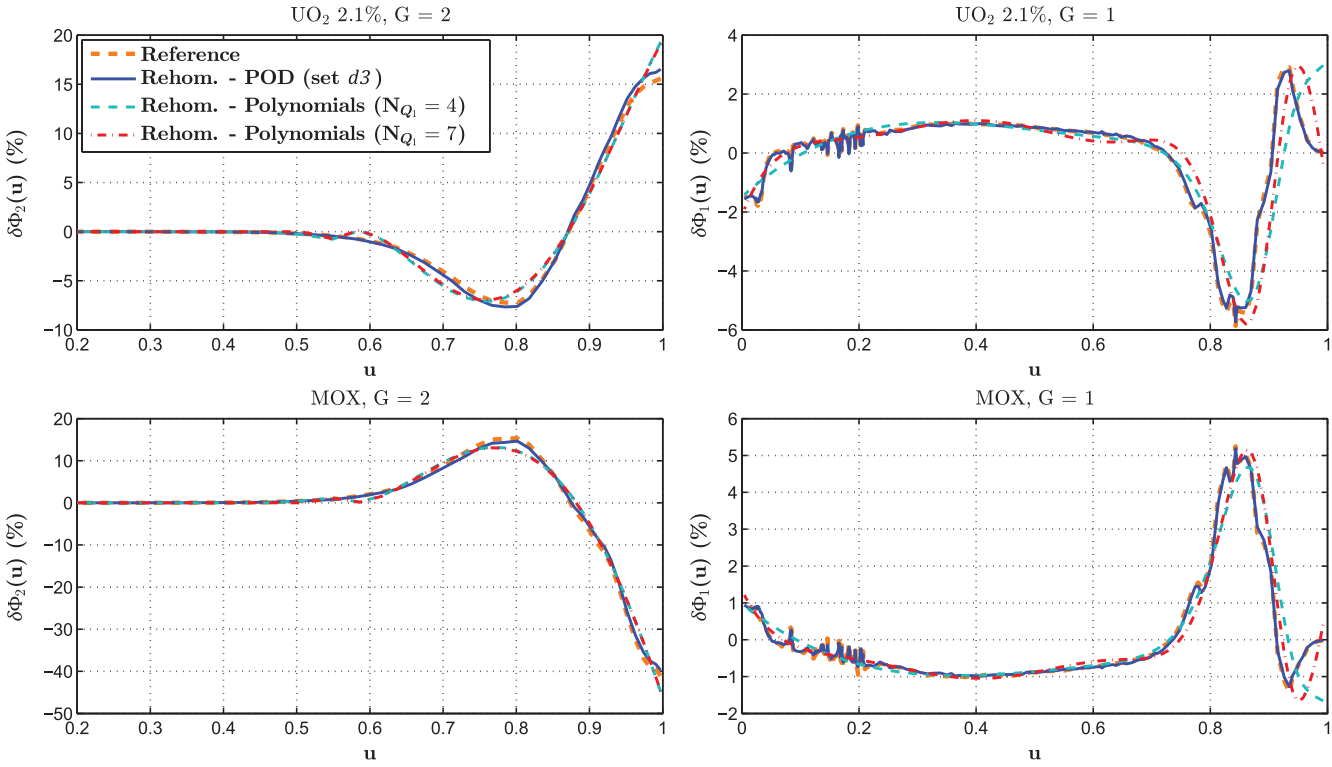


Fig. 14. Example 3: Spectrum variation per unit $u$ computed by rehomogenization.

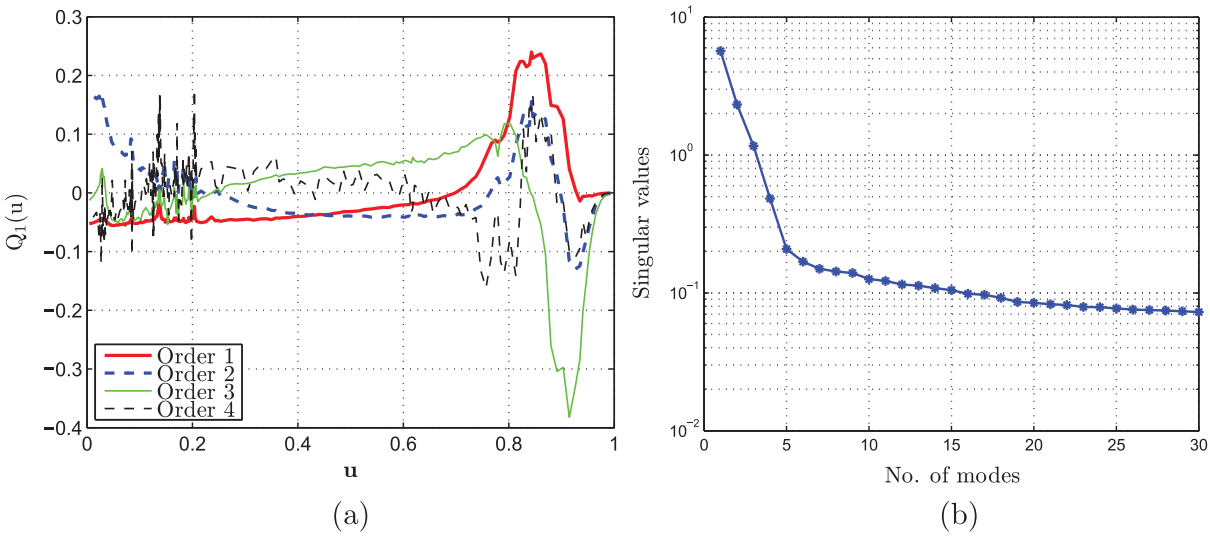


Fig. 15. (a) Fast-group POD modes computed by the SVD of the ensemble of snapshot sets built for examples 1, 2, and 3. (b) Singular values of the basis functions.

visible in the epithermal range (within $u_1 \in [0,0.1]$) for the $UO_2$ and MOX assemblies (see Fig. 14). The behavior of the singular values for the computed modes is shown in Fig. 15b. The first four basis functions have significantly higher singular values than the remaining ones. This suggests that they retain most of the information carried by the original snapshot set and that they are sufficient for an accurate reconstruction of the solution.

The polynomial-based rehomogenization with only four modes in the fast group cannot fit the bulge shape due to its strongly varying outline. The computed $\delta\Phi(u)$ exhibits a monotonic behavior until the upper pseudolethargy boundary. A misprediction in the highest part of

the spectrum affects the rehomogenization of the production cross section. Because of the fast fissions of $^{238}U$, the $\nu\Sigma_f$ distribution usually assumes its higher values for $u_1 > 0.8$ (if one does not consider the resonance spikes). Hence, the error on $\delta\Phi_1$ for $u_1 \in [0.9, 1.0]$ has more weight in the calculation of the few-group correction. A significantly better prediction is achieved increasing the number of fast-group basis functions to seven.

The errors in the integral parameters and nodal cross sections are shown in Tables VIII, IX, and X. Also in this case, a limitation of the method due to the exclusion of spatial effects is apparent: in the MOX assembly, the error on $\nu\Sigma_{f,2}$ corrected with the reference $\delta\nu\Sigma_{f,2}$ increases compared to the infinite-medium value. The same occurs for fast fission in both assemblies and for thermal absorption in the MOX bundle. We verified that the errors in $\Sigma_{a,2}$ and $\nu\Sigma_{f,2}$ in the latter assembly vanish when spectral rehomogenization is applied in combination with the reference spatial cross-section corrections. Previous considerations about the misprediction of $\delta\Phi_1$ in calculation $c1$ are confirmed by the errors in the fast-group cross sections (and fast-group nodal power).

When rehomogenization is applied, the number of power iterations increases by a factor of 1.7 and 1.9 when seven and four polynomial basis functions are used in the fast group, respectively. An increment of 2.2 is found with the POD modes from set $d3$.

## V. DISCUSSION

In this section, we address a number of aspects of interest of the method. The approximations made in its derivation are discussed, together with convergence features, computational cost, and memory requirements. Some conclusions are drawn about the comparison

TABLE VIII

Example 3: Errors in the Multiplication Factor and Nodal Fission Power

| Simulation | Number of Power Iterations | $\Delta k_{eff}$ (pcm) | $UO_2$ 2.1% | MOX |
|---|---|---|---|---|
| | | | Error on $P_{avg}$ (%) | Error on $P_{avg}$ (%) |
| Standard ($a$) | 10 | 30 | 0.73 (0.26, 0.86) | −0.55 (−0.15, −0.71) |
| Reference $\delta\Sigma^{spectr}$ ($b$) | 10 | −7 | −0.21 (0.53, −0.45) | 0.15 (−0.30, 0.38) |
| Spectral rehomogenization Chebyshev ($c1$) | 19 | 21 | −0.21 (0.92, −0.59) | 0.16 (−0.53, 0.49) |
| Spectral rehomogenization Chebyshev ($c2$) | 17 | 24 | −0.29 (0.53, −0.57) | 0.21 (−0.31, 0.47) |
| Spectral rehomogenization POD ($d1$) | 27 | −18 | −0.16 (0.31, −0.34) | −0.12 (−0.18, 0.28) |
| Spectral rehomogenization POD ($d3$) | 22 | −21 | −0.25 (0.51, −0.50) | 0.18 (−0.29, 0.42) |

TABLE IX

Example 3: Errors in the Nodal Cross Sections of the $UO_2$ Assembly

| $UO_2$ 2.1% | $\Sigma_{a,1}$ | $\Sigma_{a,2}$ | $\nu\Sigma_{f,1}$ | $\nu\Sigma_{f,2}$ | $\Sigma_{t,1}$ | $\Sigma_{t,2}$ | $\Sigma_{s,1\to1}$ | $\Sigma_{s,1\to2}$ | $\Sigma_{s,2\to2}$ |
|---|---|---|---|---|---|---|---|---|---|
| Reference ($cm^{-1}$) | 0.00927 | 0.0894 | 0.00547 | 0.0979 | 0.534 | 1.302 | 0.508 | 0.0171 | 1.211 |
| Simulation | Error (%) | | | | | | | | |
| Standard ($a$) | −0.61 | 1.12 | 0.07 | 1.27 | −0.33 | 0.53 | −0.37 | 1.18 | 0.50 |
| Reference $\delta\Sigma^{spectr}$ ($b$) | 0.11 | 0.18 | 0.35 | 0.30 | 0.01 | 0.01 | 0.01 | −0.05 | 0.0 |
| Spectral rehomogenization Chebyshev ($c1$) | 0.28 | 0.13 | 0.76 | 0.24 | 0.0 | 0.0 | 0.0 | −0.1 | −0.02 |
| Spectral rehomogenization Chebyshev ($c2$) | 0.17 | 0.23 | 0.34 | 0.33 | 0.02 | 0.07 | 0.02 | −0.08 | 0.06 |
| Spectral rehomogenization POD ($d1$) | 0.23 | 0.11 | 0.05 | 0.22 | 0.16 | −0.03 | 0.16 | 0.24 | −0.04 |
| Spectral rehomogenization POD ($d3$) | 0.05 | 0.12 | 0.31 | 0.24 | 0.0 | −0.02 | 0.0 | −0.10 | −0.03 |

TABLE X

Example 3: Errors in the Nodal Cross Sections of the MOX Assembly

| MOX | $\Sigma_{a,1}$ | $\Sigma_{a,2}$ | $\nu\Sigma_{f,1}$ | $\nu\Sigma_{f,2}$ | $\Sigma_{t,1}$ | $\Sigma_{t,2}$ | $\Sigma_{s,1\to1}$ | $\Sigma_{s,1\to2}$ | $\Sigma_{s,2\to2}$ |
|---|---|---|---|---|---|---|---|---|---|
| Reference ($cm^{-1}$) | 0.0142 | 0.260 | 0.00990 | 0.375 | 0.526 | 1.517 | 0.498 | 0.0131 | 1.254 |
| Simulation | Error (%) | | | | | | | | |
| Standard (*a*) | 0.02 | 0.42 | 0.02 | 0.58 | 0.39 | −0.64 | 0.43 | −0.87 | −0.90 |
| Reference $\delta\Sigma^{spectr}$ (*b*) | −0.08 | 0.88 | −0.25 | 1.08 | −0.01 | 0.34 | −0.01 | 0.04 | 0.23 |
| Spectral rehomogenization Chebyshev (*c1*) | −0.22 | 0.91 | −0.47 | 1.13 | 0.0 | 0.26 | 0.0 | 0.20 | 0.13 |
| Spectral rehomogenization Chebyshev (*c2*) | −0.19 | 0.82 | −0.30 | 1.04 | −0.01 | 0.16 | −0.01 | 0.20 | 0.03 |
| Spectral rehomogenization POD (*d1*) | −0.24 | 0.81 | −0.26 | 0.98 | −0.10 | 0.30 | −0.10 | −0.02 | 0.20 |
| Spectral rehomogenization POD (*d3*) | 0.0 | 0.90 | −0.25 | 1.11 | 0.0 | 0.30 | 0.0 | 0.08 | 0.17 |

between the polynomial and POD approaches for the spectrum-change synthesis. The relation between rehomogenization and the $B^2$ spectral correction is considered. Finally, a preliminary analysis on a model for the leakage spectral distribution is made.

## V.A. Remarks

### V.A.1. Approximations in the Formulation of the Method

As mentioned in Sec. II, the rehomogenization coefficients are computed with the fine-group infinite-medium cross-section distributions [Eq. (16)]. This is an approximation because Eq. (5) is rigorously valid in the real environment, where deviations of the $\Sigma(u)$ distributions occur. These are due to variations of the fuel, fission product, and burnable absorber isotopic concentrations $N_i$ with respect to the infinite-medium depletion and of the fine-group microscopic cross sections $\sigma_i(u)$. The latter are influenced by self-shielding effects in the heterogeneous arrangement of the fuel elements inside the assembly. In the core environment the flux distribution obviously changes not only at the assembly level but also at the cell and pin levels, especially in the surroundings of the border with a different region. Strong spatial perturbations of the spectrum inside the cell can cause variations of the ratio between the flux in the fuel rod and in the moderator. This results in a modification of the resonance escape probability.

In view of these considerations, as mentioned in Sec. V.A.2, a procedure for an on-the-fly update of the rehomogenization coefficients has been developed to account for changes in the nuclide content $N_i$. In this section, we briefly investigate the impact of using infinite-medium microscopic cross-section distributions in Eq. (16). We consider the $UO_2$/MOX colorset (example 3), in which the effects of within-cell flux distribution are expected to be more relevant due to the high flux gradients at the interface between the two assemblies (see Fig. 14). As shown in Fig. 16, in the MOX assembly, deviations up to 1.5% are found between the environmental and infinite-medium $\Sigma_a(u)$ distributions in the thermal range and at the highest energies of the fast group. The nuclide densities are the

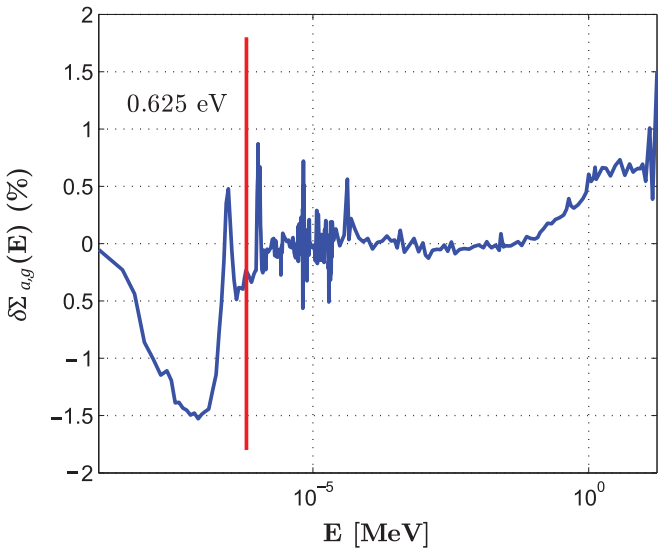


Fig. 16. Example 3: Variation of the MOX assembly absorption cross-section spectral distribution between the environmental and infinite-medium conditions.

same in the single-assembly and colorset calculations, so the only differences are due to the fine-group microscopic cross sections. The observed errors are comparable, in terms of magnitude, to those of the two-group single-assembly cross sections.

Table XI shows the results of the calculations with POD-based rehomogenization in which the $h_R$ and $h_V$ parameters (other than $h_{V,x,G,i,0}$ coefficients) have been computed with the environmental and single-assembly $\sigma(u)$ distributions. The errors $\Delta$ in the nodal power and cross sections are expressed in percentage. The differences in the nodal cross sections between the two simulations are negligible in the thermal range and small in the fast one (they mostly concern fast-group absorption). The deviations in the integral parameters are also not relevant. This outcome is because variations in the fine-group microscopic cross sections are considerably smaller than variations in the spectrum, which have a larger effect. A similar outcome has been found for the remaining test cases considered in this work. Hence, it may be concluded that the use of the infinite-lattice $\sigma(u)$ distributions in the calculation of the $h_{R,x,G,j}$ and $h_{V,x,G,i,j}$ coefficients (with $j \neq 0$) does not affect the performance of the method. We remark that it is mathematically consistent to use the infinite-medium distributions in Eqs. (3) and (17) (i.e., for $j = 0$) due to the derivation made in our previous work.[21]

Another approximation of the method is that the cross-section corrections are averaged over the node, whereas in reality the magnitude of the spectral effects is significantly higher at the interface with the neighbor assemblies. For the $UO_2$-MOX interface of example 3, Fig. 17 shows the reference spectrum variation (per unit of standard lethargy) in the $UO_2$ bundle as a function of the distance from the assembly edge. The magnitude of the node-averaged perturbation corresponds to that observed approximately 3 cm away from the assembly border (that is, within the third row of fuel cells). The high spatial gradients in the spectrum change suggest that mixed space-energy terms (currently neglected by the method) can be important and should be modeled.

As a final remark, this rehomogenization approach does not correct the few-group discontinuity factors, which depend by definition on heterogeneous spatial form functions. Since our approach relies on assembly-averaged distributions, a rigorous way has not been found so far to determine a spectral correction for this kind of homogenization parameter. However, a correction on the discontinuity factors is computed by the spatial rehomogenization method that has been developed in parallel to the spectral one.[6]

TABLE XI

Example 3: Effect of the Environment on the Rehomogenization Coefficients

| Simulation | $\Delta k_{eff}$ (pcm) | $UO_2$ 2.1% | | | | | MOX | | | | |
|---|---|---|---|---|---|---|---|---|---|---|---|
| | | $\Delta P_{avg}$ | $\Delta\Sigma_{a,1}$ | $\Delta\Sigma_{a,2}$ | $\Delta\nu\Sigma_{f,1}$ | $\Delta\nu\Sigma_{f,2}$ | $\Delta P_{avg}$ | $\Delta\Sigma_{a,1}$ | $\Delta\Sigma_{a,2}$ | $\Delta\nu\Sigma_{f,1}$ | $\Delta\nu\Sigma_{f,2}$ |
| $h_R$, $h_V$ from $\Sigma^{\infty}_{x,G}(u)$ | −21 | −0.25 (0.51, −0.50) | 0.05 | 0.12 | 0.31 | 0.24 | 0.18 (−0.29, 0.42) | 0.0 | 0.90 | −0.25 | 1.11 |
| $h_R$, $h_V$ from $\Sigma^{env}_{x,G}(u)$ | −39 | −0.30 (0.48, −0.58) | 0.20 | 0.14 | 0.41 | 0.25 | 0.23 (−0.28, 0.48) | 0.29 | 0.85 | −0.12 | 1.04 |

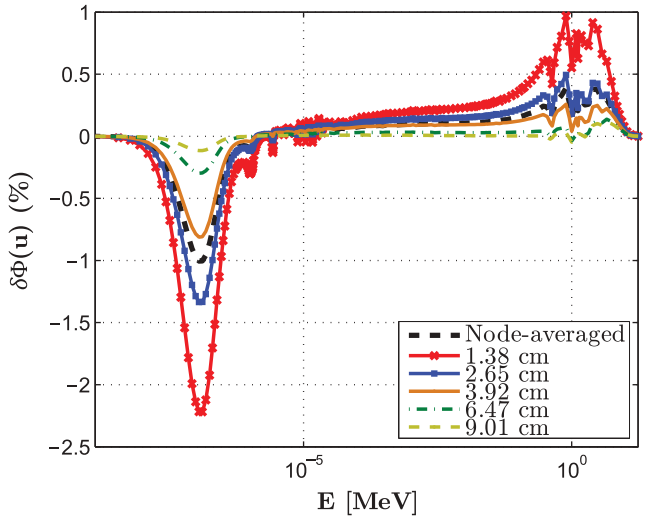


Fig. 17. $UO_2$-MOX interface: spectrum perturbation (per unit lethargy) in the $UO_2$ bundle as a function of the distance from the assembly edge. The percent variation is referred to the assembly-averaged total (i.e., one-group) flux.

### V.A.2. Implementation Features and Calculational Efficiency

In order to dampen numerical oscillations occurring with Galerkin projection, an underrelaxation factor θ has been introduced for the spectrum variation. Hence, at each rehomogenization update $m$, the computed expansion coefficients $\alpha^m_{G,i}$ are corrected as follows:

$$\alpha^{m'}_{G,i} = \theta\alpha^m_{G,i} + (1-\theta)\alpha^{(m-1)'}_{G,i}, \tag{31}$$

where $\alpha^{(m-1)'}_{G,i}$ is the estimate from the previous iteration. This feature demands to store the coefficients $\alpha_{G,i}$ for each node of the domain (this is the only significant memory requirement of the method at the online calculation level). An optimal underrelaxation factor $\theta = 0.5$ has been found.

According to the calculational scheme of Fig. 5, the iterations between the nodal-flux solution and the spectral rehomogenization problem are nested in the thermal-hydraulic and depletion feedback updates. Therefore, their cost is amortized. As shown in Sec. IV.B, for the case with no feedbacks, the method produces an increase in the number of nonlinear iterations by a factor between 1.7 and 1.9 with the polynomial synthesis and between 2 and 2.8 with the POD approach. We deem that this loss of computational efficiency is fully compensated by the observed gain in accuracy. For the final application of the methodology (i.e., with a leakage model based on nodal information and feedbacks included), our goal is to limit the increment in running time with respect to a standard nodal calculation below a factor of 2.

The memory requirement for the storage of the $h_R$ and $h_V$ coefficients in the cross-section libraries can be easily quantified. We consider $\chi(u) = 0$ along the whole thermal-group energy domain (which trivially results in $\chi_{2,j} = 0, \forall j$), and we define the removal coefficients $h_{R,r,G,j} = h_{R,t,G,j} - h_{R,s,G\to G,j}$ and $h_{V,r,G,i,j} = h_{V,t,G,i,j} - h_{V,s,G\to G,i,j}$. With this choice, for a generic point in the state-parameter space, the total number of rehomogenization entries to be tabulated is given by $\sum_{G=1}^{N_G}(2N^2_{Q_G} + 7N_{Q_G}) + N_{Q_1} + N_G$. In a two-group framework and using four basis functions in each coarse group ($N_{Q_G} = 4$), this translates into 126 coefficients. In order to limit the library growth, a method has been developed to store the rehomogenization parameters only as a function of burnup. It consists of an on-the-fly update to account for the differences between the local values of moderator density, soluble-boron and xenon concentrations, and the predetermined table-point values at which the spectral coefficients are computed. This is accomplished by defining the isotopic rehomogenization coefficients for $H_2O$, $^{10}B$, and $^{135}Xe$. The method has been successfully tested in AREVA NP's ARTEMIS nodal code.[37] Its description will be addressed in future publications.

### V.A.3. About the Comparison of the Modal Approaches

The results presented in Sec. IV.B showed that the POD modes reconstruct the reference spectrum variation very accurately. Because of their capability of inheriting properties of the snapshots, they can also faithfully reproduce the details of the transport solution, such as resonance absorption spikes. In the thermal group, the spectrum perturbation is a smooth function and exhibits a very similar outline for different assembly-interface types. As a result, the thermal POD modes computed for a few test cases can be easily generalized to other configurations. On the other hand, in the fast group the spectrum deformation can contain significantly different components depending on the assembly interface. Hence, the POD basis functions have to be properly trained to capture a number of them. Purely mathematical modes can only fit the global behavior of the spectrum change. When local (energy-wise), strongly varying components are present (such as for the $UO_2$-MOX interface), they fail to reconstruct satisfactorily the shape of the

perturbation in the fast group. The use of more basis functions in this energy range can attenuate such deficiency. However, for some test cases this option has been found to cause unphysical oscillations in the $\delta\Phi$ solution when leakage form functions other than the reference one are used. Limiting the number of modes to four is thus advisable. In all the benchmark problems examined in Sec. IV.B, the nodal calculation with POD-based rehomogenization converges more slowly than that with the polynomial-based approach.

Another feature of interest in the comparison between the two strategies is the conditioning of the spectral rehomogenization problem. For the simulations of example 1, Table XII reports the condition number $C_A$ of the solving matrix corresponding to the two assemblies. The problem formulated with the POD modes is significantly better conditioned thanks to their orthonormality properties. In order to avoid numerical instabilities, the polynomial basis functions should be orthonormalized by the stabilized Gram-Schmidt process.[38] With this transformation, the rehomogenization linear system has a condition number of the same order of magnitude as that achieved with the POD operators.

In this work, we have limited our analysis on the POD approach to the calculation of sets of modes for a few relevant configurations. In order to exploit the POD-based rehomogenization at an industrial level, one has to find a set of proper orthonormal basis functions effectively usable for several assembly-interface types. Therefore, a more extensive research of snapshots has to be performed. As the number of snapshots fixes the computational burden of the POD off-line phase, and on the other hand, limits the achievable knowledge of the spectrum-change components, an effective sampling strategy has to be developed. This would have the advantage of reducing the amount of costly computations and of boosting the capability of the POD basis to reproduce the solution of problems not included in the snapshot set. In previous work,[32] we highlighted that the POD modes have a weak dependence on state parameters other than burnup. Moreover, we showed that some helpful insight into the snapshot selection process can be given by the analysis of the singular values of the snapshot matrices $A_1$ and $A_2$ [Eq. (26)]. We believe that the search of a more general set of modes can be tackled by combining an adaptive approach for the retention of snapshots (based on the singular-value decreasing importance) with a suitable numerical technique (such as sparse grids[39]) for the representation of high-dimensional functions.

TABLE XII

Example 1: Condition Number of the Assembly-Rehomogenization Linear System

| $C_A$ | $UO_2$ 1.8% | $UO_2$ 3.1% + 16 Burnable Poison Rods |
|---|---|---|
| Chebyshev | 437 792 | 439 739 |
| POD | 91 | 96 |
| Chebyshev (Gram-Schmidt) | 324 | 341 |

## V.B. Relation with the $B^2$ Correction

In this section an analysis is made on the interplay between our spectral rehomogenization method and another type of spectral cross-section correction: the critical-buckling $B^2$ correction.

In the framework of single-assembly transport calculations, it is common practice to adjust the neutron-leakage rate in the homogenized assembly to enforce a multiplication factor equal to unity.[40] This is accomplished by adding an artificial leakage cross section $\Sigma_{leak,g}$ to the fine-group absorption cross section. Such additional cross section is defined as

$$\Sigma_{leak,g} = D_g B^2 \ , \tag{32}$$

where $D_g$ is the leakage coefficient of group $g$ and $B^2$ is the buckling coefficient fulfilling the condition $k_\infty = 1$. In this way, the cross-section distributions can be collapsed with a more realistic spectrum, i.e., a spectrum closer to that of the critical core. The calculation of $B^2$ is based on the fundamental-mode assumption and is usually performed using a $B_1$ homogeneous method.[40] Refined approaches consider the space and energy dependence of the buckling coefficient.[41,42] Even if this type of correction is meant to reduce the spectral differences between the infinite medium and the core environment, it cannot reproduce in any way the spectral effects caused by unlike neighbors. It is therefore of interest to verify whether or not a relation of complementarity exists between this kind of cross-section correction and the one computed by rehomogenization.

For the analysis, we consider a rodded configuration similar to that modeled in example 2 (Sec. IV.B.2), consisting of a $UO_2$ assembly with 1.8% enrichment next to another $UO_2$ assembly with 2.4% enrichment and

24 AIC-type control rods. In order to be consistent with the fundamental-buckling approach, we study the critical-colorset configuration, achieved with a diluted-boron concentration of 222 ppm. We compare the results of the nodal calculations having the following cross-section inputs:

1. infinite-medium cross sections without $B^2$ correction ($a$)
2. infinite-medium cross sections with $B^2$ correction ($b$)
3. cross sections rehomogenized by the $\delta\Sigma_G$ computed with the reference spectrum variation $\delta\Phi_G = \Phi_{env,G} - \Phi_{\infty,G}$ ($c$)
4. cross sections rehomogenized by the $\delta\Sigma_G$ computed with the reference spectrum variation $\delta\Phi_G^{B^2} = \Phi_{env,G} - \Phi_{\infty,G}^{B^2}$ ($d$).

By $\Phi_{\infty,G}$ and $\Phi_{\infty,G}^{B^2}$, we denote the noncritical and critical (i.e., $B^2$-corrected) infinite-medium spectra, respectively. The single-assembly and colorset transport calculations for the present analysis are performed with the APOLLO2-A deterministic lattice transport code.[43] This choice allows us to avoid the computational burden of a 281-group $B_1$ spectrum calculation in SERPENT.

APOLLO2-A features two approaches for the calculation of the diffusion coefficient: the outflow transport approximation[36] and the $B_1$ method.[40] The former is the only option when single-assembly calculations are performed without critical buckling and is therefore chosen for this analysis. If no $B^2$ correction is performed, the values of $k_\infty$ in the unrodded and rodded assemblies are 1.16433 and 0.82913, respectively. Criticality is achieved with $B^2 = 0.002608$ in the former and with $B^2 = -0.003083$ in the latter.

Figure 18 shows, for the unrodded assembly, the overall spectrum variation (per unit of standard lethargy) between the critical-colorset environment and the critical and noncritical infinite lattices. The environmental and infinite-lattice spectra are normalized to unity. Clearly, the perturbation has lower magnitude when it is computed with respect to the buckling-corrected spectrum, especially for high energies. This can be explained by observing that given a positive value of $B^2$ (i.e., an outgoing neutron flow), the differences between the critical and noncritical infinite-medium spectra depend on two effects going in opposite directions: the higher leakage rate in the fast range (which tends to thermalize the spectrum) and the lower number of fast neutrons available for being scattered to thermal energies (which hardens the spectrum). The second effect is preeminent: with the $B^2$ correction, the

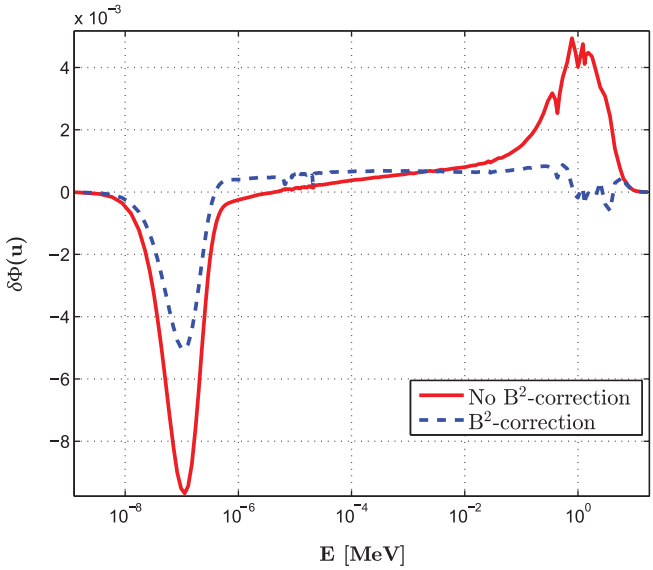


Fig. 18. Critical colorset $UO_2$ (1.8%-enriched)/$UO_2$ (2.4%-enriched) + 24 AIC control rods: unrodded-assembly spectrum change in the real environment with respect to the critical and noncritical infinite lattices. The neutron spectra are normalized to unity.

spectral index in the unrodded assembly increases from 3.304 to 3.482. Since the spectrum is hardened by the assembly with control rods in the colorset environment, the spectrum variation is attenuated by the $B^2$ correction.

Table XIII shows the errors in the integral parameters and nodal cross sections for calculations $a$, $b$, $c$, and $d$. The deviations in the nodal power and cross sections are expressed in percentage. Comparing simulations $a$ and $b$, it appears that the $B^2$ correction significantly reduces the errors in the fast production and fast-to-thermal scattering cross sections, whereas it considerably overcorrects the fast absorption and fast total cross sections. As thermal neutrons are much less "leakage-prone," the correction has little influence on the thermal cross sections. The calculation with buckling exhibits significantly lower errors in the nodal power but a much higher error in $k_{eff}$. In calculations $c$ and $d$, the errors are very close. The differences in the nodal cross sections between the two simulations (observable, for instance, in the error in fast fission) lie within the range of accuracy of the calculation. The same holds for the errors in $k_{eff}$ and in the nodal power. This suggests that rehomogenization is not influenced by the fact that the infinite-medium cross sections are generated at conditions very far from criticality (16 433 pcm off criticality in the unrodded assembly, −17 087 pcm off criticality in the rodded one). Apparently, the method can reproduce both neighbor effects (which cannot be modeled by the $B^2$

TABLE XIII

Effect of the $B^2$ Correction on the Calculations Without and With Rehomogenization

| Simulation | $\Delta k_{eff}$ (pcm) | $UO_2$ 1.8% | | | | $UO_2$ 2.4% + 24 AIC Rods | | | | |
|---|---|---|---|---|---|---|---|---|---|---|
| | | $\Delta P_{avg}$ | $\Delta\Sigma_{a,1}$ | $\Delta\Sigma_{a,2}$ | $\Delta\nu\Sigma_{f,1}$ | $\Delta\nu\Sigma_{f,2}$ | $\Delta P_{avg}$ | $\Delta\Sigma_{a,1}$ | $\Delta\Sigma_{a,2}$ | $\Delta\nu\Sigma_{f,1}$ | $\Delta\nu\Sigma_{f,2}$ |
| Standard (no $B^2$ correction) (*a*) | −171 | 3.28 (1.34, 3.67) | 1.06 | 0.77 | 0.66 | 0.85 | −4.19 (−1.28, −5.02) | −1.19 | 0.54 | −0.93 | −1.33 |
| Standard ($B^2$ correction) (*b*) | −617 | 1.42 (0.48, 1.63) | −0.72 | 0.66 | 0.11 | 0.72 | −1.81 (−0.46, −2.23) | 1.31 | 0.63 | 0.10 | −1.21 |
| Reference $\delta\Sigma^{spectr}$ (no $B^2$ correction) (*c*) | −453 | 1.31 (0.49, 1.49) | 0.06 | 0.24 | −0.05 | 0.29 | −1.68 (−0.47, −2.04) | 0.30 | 1.43 | 0.05 | −0.14 |
| Reference $\delta\Sigma^{spectr}$ ($B^2$ correction) (*d*) | −458 | 1.27 (0.44, 1.45) | 0.06 | 0.21 | 0.12 | 0.26 | −1.61 (−0.42, −1.98) | 0.34 | 1.45 | −0.09 | −0.11 |

correction) and spectral effects due to different physical conditions between the core environment and the infinite lattice (i.e., different multiplicative properties). Therefore, the two corrections are not complementary.

Although the fundamental-buckling correction is widely adopted in the preparation of cross-section libraries, its application is notoriously not rigorous when simulating noncritical conditions in which the spectrum differs from the critical one.[44–46] These include reactor core transients and subcritical states during power outage. For example, in Ref. 46 it is shown that the use of $B^2$-tweaked cross sections can have a large impact on the nodal simulation of transients strongly deviating from criticality. Spectral rehomogenization makes the critical-buckling procedure redundant. Thus, the $B^2$ approach can be eliminated from the preparation of the cross-section libraries. In this way, no bias is introduced in the simulation of noncritical conditions, and one of the limitations in the current methodology for cross-section generation is removed (with an advantage also in terms of the computational cost of the lattice calculation).

## V.C. A Model for the Leakage Spectral Distribution

In the calculations performed in this paper, the leakage energy distribution from the reference transport solution has been used in the rehomogenization problem. In the final implementation of the methodology, this shape is to be computed on the basis of nodal information.

In a preliminary attempt, a flat-leakage approximation was used, setting $L_{env,G}(u)$ equal to the few-group nodal value $\bar{L}_G$ [i.e., $f_{L,G}(u) = 1$ in Eq. (11)]. This approach was tested in combination with step functions as weighting operators for the rehomogenization problem (under the assumption of a constant leakage distribution, the use of Galerkin weighting with zero-averaged basis functions would result in $c_{G,j} = 0$). Not surprisingly, this rough approximation gave poor results and had to be abandoned.

The leakage-projection coefficient $c_{G,j}$ [Eq. (16a)] can be computed using information from the fine-group lattice transport calculation. In this case, the form function approximating the environmental leakage has to be prescribed a priori or defined as a function of infinite-medium quantities that are known a priori. A possibility is to use the infinite-medium fundamental-leakage distribution $f^{\infty}_{L,G}$. We define it, with normalization to unity, as

$$f^{\infty}_{L,G}(u) = \frac{DB^2(u)\varphi_{\infty,G}(u)}{\int_0^1 du DB^2(u)\varphi_{\infty,G}(u)} . \quad (33)$$

This straightforward approach avoids formulating more complex models. However, the leakage distribution in the real environment can differ significantly from that in the infinite-medium critical assembly. Moreover, such strategy can be used only with $B^2$-corrected cross-section libraries. Hence, it lacks generality, and it might suffer from the deficiencies of the $B_1$ calculation highlighted in Sec. V.B.

An alternative method that has been recently developed is based on the application of Fick's law to the neutron spectra. The local leakage shape is thus defined as a function of the difference between the environmental spectrum in the node and the environmental spectra in the surrounding nodes. According to this diffusive approach, the leakage spectral distribution $f_{L,G}^{k,diff}$ at the interface $kl$ between two adjacent nodes $k$ and $l$ is formulated for node $k$ as follows:

$$f_{L,G}^{k,diff}(u) = c_G^k \bar{D}_G^{kl}(u)(\Phi_{env,G}^k(u) - \Phi_{env,G}^l(u)) \ , \qquad (34)$$

where

$c_G^k$ = normalization constant

$\bar{D}_G^{kl}(u)$ = average diffusion coefficient

$\Phi_{env,G}^m(u)$ (with $m = k, l$) = environmental spectrum in node $m$ computed by rehomogenization.

This nonlinear strategy has given very accurate results for several benchmark problems and is so far the best candidate for the final implementation in the ARTEMIS code.[37] For example, Fig. 19 shows the fast-group leakage distributions computed with the fundamental-mode and diffusive approaches for the unrodded assembly of example 2 (Sec. IV.B.2). From the comparison with the reference environmental leakage, it emerges that the second method gives a very accurate approximation, especially in the epithermal region of the spectrum.

Other approaches have been investigated, including a modal synthesis of the leakage form function. A thorough description of these models is deferred for subsequent publication.

## VI. CONCLUSIONS

In this work, we have presented an on-the-fly modal-synthesis method for spectral rehomogenization of nodal cross sections. The approach has a physical foundation. This feature distinguishes it from other spectral-correction methods available in literature, most of which resort to empirical correlations and to the tabulation of precalculated corrections.

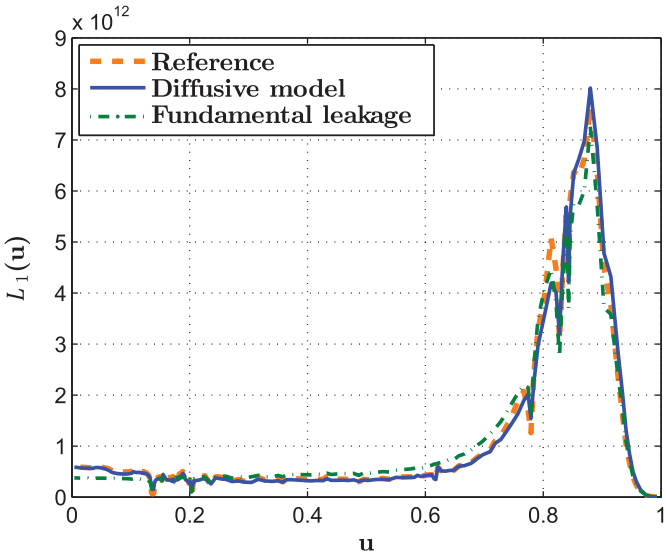


Fig. 19. Example 2: Fast-group leakage spectrum in the unrodded assembly, computed with a nonlinear diffusive model and with the fundamental-mode approximation [in units of neutrons/(cubic centimeters · second)].

The method has been validated for assembly configurations typically encountered in PWR cores. The case with no thermal or depletion feedbacks has been considered. Focus has been given to the definition of effective sets of basis and weighting functions for the environmental spectrum reconstruction. The rehomogenization algorithm can reproduce very accurately the spectral effects on the cross sections when the reference leakage energy distribution is used. The results of a model for the leakage spectrum, relying on nodal information and lattice-calculation data, are also promising. The method has an acceptable computational burden, and the changes to the cross-section parameterized tables merely consist of the inclusion of additional homogenization coefficients. Another benefit is that the $B_1$ critical-spectrum correction is no longer needed.

A limitation of this approach is that it can only correct a part of the homogenization error. In order to fully capture core-environment effects, it cannot be decoupled from an effective spatial rehomogenization. Based on the results presented in this paper, a combined spatial and spectral rehomogenization scheme may contribute to obtain significantly more accurate estimates of LWR power distribution and multiplication factor from nodal diffusion codes still using the single-assembly homogenization paradigm.

Future work will include the validation of the leakage spectral model and the application of the methodology to configurations with thermal hydraulics and depletion feedbacks and to whole-core calculations. It will be demonstrated that this approach can model spectral effects associated with

not only interassembly heterogeneity but also local changes in the nuclide densities. This feature might be exploited to devise a rehomogenization-based cross-section model in which the interpolation of the cross sections versus state parameters other than burnup and fuel temperature is removed. Other topics to be addressed are the analysis on boiling-water-reactor assembly configurations and the extension of the POD approach to industrial calculations. Finally, an investigation of the effect of the spatial discretization on the method is of great interest, with particular attention to applications in the context of pin-by-pin calculations.

## Acknowledgment

This work was supported by the AREVA PhD program.

## ORCID

Matteo Gamarino http://orcid.org/0000-0001-8074-5931

## References

1. R. D. LAWRENCE, "Progress in Nodal Methods for the Solution of the Neutron Diffusion and Transport Equations," *Prog. Nucl. Energy*, **17**, *3*, 271 (1986); https://doi.org/10.1016/0149-1970(86)90034-X.
2. W. M. STACEY, *Nuclear Reactor Physics*, John Wiley & Sons (2007).
3. K. S. SMITH, "Assembly Homogenization Techniques for Light Water Reactor Analysis," *Prog. Nucl. Energy*, **17**, *3*, 303 (1986); https://doi.org/10.1016/0149-1970(86)90035-1.
4. K. S. SMITH, "Practical and Efficient Iterative Method for LWR Fuel Assembly Homogenization," *Trans. Am. Nucl. Soc.*, **71**, 238 (1994).
5. T. BAHADIR and S.-Ö. LINDAHL, "Studsvik's Next Generation Nodal Code SIMULATE-5," *Proc. Advances in Nuclear Fuel Management (ANFM IV)*, Hilton Head, South Carolina, April 12–15, 2009, American Nuclear Society (2009).
6. A. DALL'OSSO, "Spatial Rehomogenization of Cross Sections and Discontinuity Factors for Nodal Calculations," *Proc. Int. Conf. PHYSOR*, Kyoto, Japan, September 28–October 3, 2014.
7. M. R. WAGNER, K. KOEBKE, and H.-J. WINTER, "A Non-Linear Extension of the Nodal Expansion Method," *Proc. Int. Topl. Mtg. Advances in Mathematical Methods for the Solution of Engineering Problems*, Munich, Germany, April 27–29, 1981, Vol. 2 (1981).
8. P. FORSLUND, E. MÜLLER, and S.-Ö. LINDAHL, "Investigation of Intranodal Depletion Effects," *Ann. Nucl. Energy*, **28**, *3*, 225 (2001); https://doi.org/10.1016/S0306-4549(00)00043-8.
9. Y. SHATILLA, Y. CHAO, and Y. TAHARA, "Theory of Westinghouse Advanced Nodal Code for MOX Applications," *Trans. Am. Nucl. Soc.*, **75**, 168 (1996).
10. S. P. PALMTAG, "Advanced Nodal Methods for MOX Fuel Analysis," PhD Thesis, Massachusetts Institute of Technology (1997).
11. Y. BAN and H. JOO, "Leakage Correction of Homogenized Few-GCS Through Functionalization on Leakage Fraction," *Proc. Int. Topl. Mtg. Reactor Physics (PHYSOR)*, Sun Valley, Idaho, May 1–5, 2016, p. 1815, American Nuclear Society (2016).
12. F. RAHNEMA and E. M. NICHITA, "Leakage Corrected Spatial (Assembly) Homogenization Technique," *Ann. Nucl. Energy*, **24**, *6*, 477 (1997); https://doi.org/10.1016/S0306-4549(96)00084-9.
13. W. KIM, W. HEO, and Y. KIM, "Improvement of Nodal Accuracy by Using Albedo-Corrected Parameterized Equivalence Constants," *Nucl. Sci. Eng.*, **188**, *3*, 207 (2017); https://doi.org/10.1080/00295639.2017.1354592.
14. K. T. CLARNO and M. L. ADAMS, "Capturing the Effects of Unlike Neighbors in Single-Assembly Calculations," *Nucl. Sci. Eng.*, **149**, *2*, 182 (2005); https://doi.org/10.13182/NSE04-31.
15. F. RAHNEMA and M. S. McKINLEY, "High-Order Cross-Section Homogenization Method," *Ann. Nucl. Energy*, **29**, *7*, 875 (2002); https://doi.org/10.1016/S0306-4549(01)00079-2.
16. M. S. McKINLEY and F. RAHNEMA, "Higher-Order Boundary Condition Perturbation Theory for the Diffusion Approximation," *Nucl. Sci. Eng.*, **136**, *1*, 15 (2000); https://doi.org/10.13182/NSE00-A2145.
17. M. S. McKINLEY and F. RAHNEMA, "High-Order Boundary Condition Perturbation Theory for the Neutron Transport Equation," *Nucl. Sci. Eng.*, **140**, *3*, 285 (2002); https://doi.org/10.13182/NSE02-A2261.
18. L. ZHU and B. FORGET, "An Energy Recondensation Method Using the Discrete Generalized Multigroup Energy Expansion Theory," *Ann. Nucl. Energy*, **38**, *8*, 1718 (2011); https://doi.org/10.1016/j.anucene.2011.04.008.
19. S. GROENEWALD, R. PRINSLOO, and O. ZAMONSKY, "Practical Semi-Heterogeneous Method in Nodal Core Analysis," *Proc. Int. Conf. Mathematics and Computational Methods Applied to Nuclear Science and Engineering (M&C 2017)*, Jeju, Korea, April 16–20, 2017.
20. A. DALL'OSSO, D. TOMATIS, and Y. DU, "Improving Cross Sections via Spectral Rehomogenization," *Proc. Int. Conf. PHYSOR 2010*, Pittsburgh, Pennsylvania, May 9–14, 2010, American Nuclear Society (2010).

21. M. GAMARINO et al., "Investigation of Rehomogenization in the Framework of Nodal Cross Section Corrections," *Proc. Int. Topl. Mtg. Reactor Physics (PHYSOR)*, Sun Valley, Idaho, May 1–5, 2016, p. 3698, American Nuclear Society (2016).

22. W. M. STACEY, *Modal Approximations: Theory and an Application to Reactor Physics*, Vol. 41, MIT Press (1967).

23. A. DALL'OSSO, "Introducing the Migration Mode Method for the Solution of the Space and Energy Dependent Diffusion Equation," *Ann. Nucl. Energy*, **30**, *18*, 1829 (2003); https://doi.org/10.1016/S0306-4549(03)00157-9.

24. J. LAMARSH, *Introduction to Nuclear Reactor Theory*, Addison-Wesley, Reading, Massachusetts (1966).

25. A. GANDINI, "A Generalized Perturbation Method for Bi-Linear Functionals of the Real and Adjoint Neutron Fluxes," *J. Nucl. Energy*, **21**, *10*, 755 (1967); https://doi.org/10.1016/0022-3107(67)90086-X.

26. A. CHATTERJEE, "An Introduction to the Proper Orthogonal Decomposition," *Curr. Sci.*, **78**, *7*, 808 (2000).

27. K. KUNISCH and S. VOLKWEIN, "Galerkin Proper Orthogonal Decomposition Methods for Parabolic Problems," *Numer. Math.*, **90**, *1*, 117 (2001); https://doi.org/10.1007/s002110100282.

28. F. WOLS, "Transient Analyses of Accelerator Driven Systems Using Modal Expansion Techniques," Master's Thesis, Delft University of Technology (2010).

29. A. SARTORI, "Reduced Order Methods: Applications to Nuclear Reactor Core Spatial Dynamics," PhD Thesis, Politecnico di Milano (2015).

30. A. BUCHAN et al., "A POD Reduced-Order Model for Eigenvalue Problems with Application to Reactor Physics," *Int. J. Numer. Methods Eng.*, **95**, *12*, 1011 (2013); https://doi.org/10.1002/nme.4533.

31. A. G. BUCHAN et al., "A POD Reduced Order Model for Resolving Angular Direction in Neutron/Photon Transport Problems," *J. Comput. Phys.*, **296**, 138 (2015); https://doi.org/10.1016/j.jcp.2015.04.043.

32. M. GAMARINO et al., "Spectral Rehomogenization of Nodal Cross-Sections via Proper Orthogonal Decomposition," *Proc. Int. Conf. Mathematics and Computational Methods Applied to Nuclear Science and Engineering (M&C 2017)*, Jeju, Korea, April 16–20, 2017.

33. J. LEPPÄNEN et al., "The Serpent Monte Carlo Code: Status, Development and Applications in 2013," *Ann. Nucl. Energy*, **82**, 142 (2015); https://doi.org/10.1016/j.anucene.2014.08.024.

34. A. KONING et al., "The JEFF-3.1 Nuclear Data Library," Organisation for Economic Co-operation and Development (2006).

35. Z. LIU, K. SMITH, and B. FORGET, "A Cumulative Migration Method for Computing Rigorous Transport Cross Sections and Diffusion Coefficients for LWR Lattices with Monte Carlo," *Proc. Int. Topl. Mtg. Reactor Physics (PHYSOR)*, Sun Valley, Idaho, May 1–5, 2016, p. 2915, American Nuclear Society (2016).

36. S. CHOI et al., "Impact of Inflow Transport Approximation on Light Water Reactor Analysis," *J. Comput. Phys.*, **299**, 352 (2015); https://doi.org/10.1016/j.jcp.2015.07.005.

37. G. HOBSON et al., "ARTEMIS$^{TM}$ Core Simulator: Latest Developments," *Proc. Joint Int. Conf. Supercomputing in Nuclear Applications+Monte Carlo (SNA+MC 2013)*, Paris, France, October 27–31, 2013, EDP Sciences (2014).

38. G. H. GOLUB and C. F. VAN LOAN, *Matrix Computations*, Vol. 3, JHU Press (2012).

39. H.-J. BUNGARTZ and M. GRIEBEL, "Sparse Grids," *Acta Numerica*, **13**, 147 (2004); https://doi.org/10.1017/S0962492904000182.

40. A. HEBERT, *Applied Reactor Physics*, Presses Internationales Polytechnique (2009).

41. P. BENOIST, J. MONDOT, and I. PETROVIC, "Calculational and Experimental Investigations of Void Effect – A Simple Theoretical Model for Space-Dependent Leakage Treatment of Heterogeneous Assemblies," *Nucl. Sci. Eng.*, **118**, *4*, 197 (1994); https://doi.org/10.13182/NSE94-A21491.

42. K. SMITH, "Nodal Diffusion Methods: Understanding Numerous Unpublished Details," *Proc. Int. Topl. Mtg. Reactor Physics (PHYSOR)*, Sun Valley, Idaho, May 1–5, 2016, p. 1227, American Nuclear Society (2016).

43. E. MARTINOLLI et al., "APOLLO2-A – AREVA's New Generation Lattice Physics Code: Methodology and Validation," *Proc. Int. Conf. PHYSOR 2010*, Pittsburgh, Pennsylvania, May 9–14, 2010, American Nuclear Society (2010).

44. A. DALL'OSSO, "Neutron Spectrum Kinetics in the Infinite Homogeneous Reactor," *Ann. Nucl. Energy*, **85**, 662 (2015); https://doi.org/10.1016/j.anucene.2015.06.022.

45. A. DALL'OSSO, "The Influence of the Neutron Source Spectrum on the Infinite Homogeneous Reactor in Subcritical Condition," *Ann. Nucl. Energy*, **77**, 408 (2015); https://doi.org/10.1016/j.anucene.2014.12.006.

46. C. DEMAZIÈRE, "Investigation of the Bias Coming from Spectrum Corrections in the Simulations of Nuclear Reactor Transients," *Proc. Int. Topl. Mtg. Reactor Physics (PHYSOR)*, Sun Valley, Idaho, May 1–5, 2016, p. 3561, American Nuclear Society (2016).